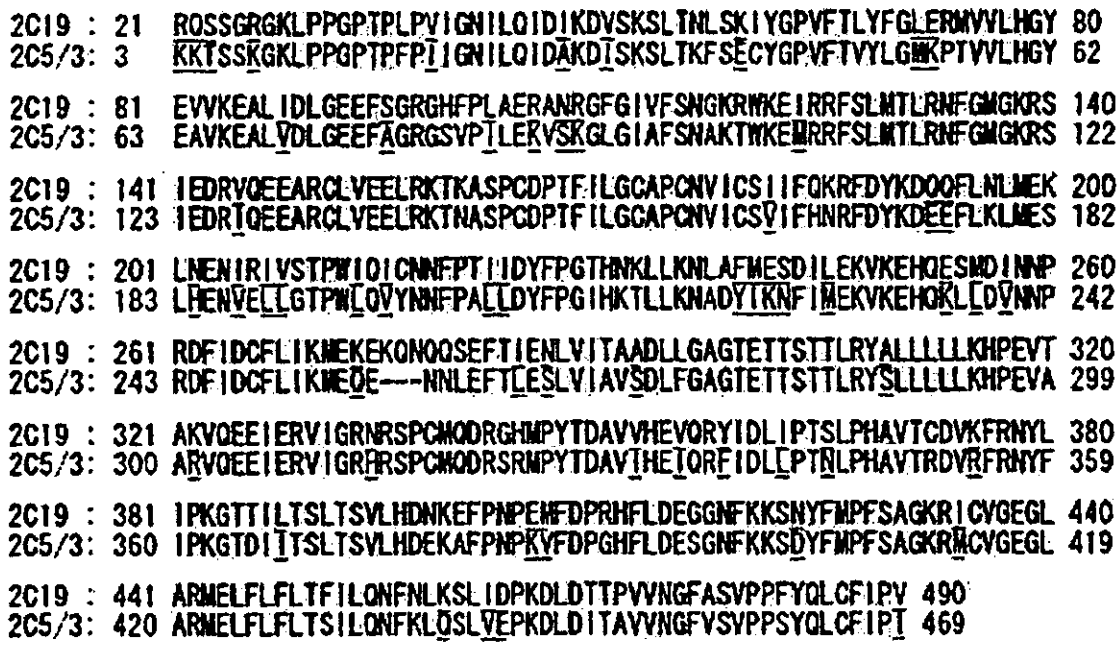

(a) CYP2C19

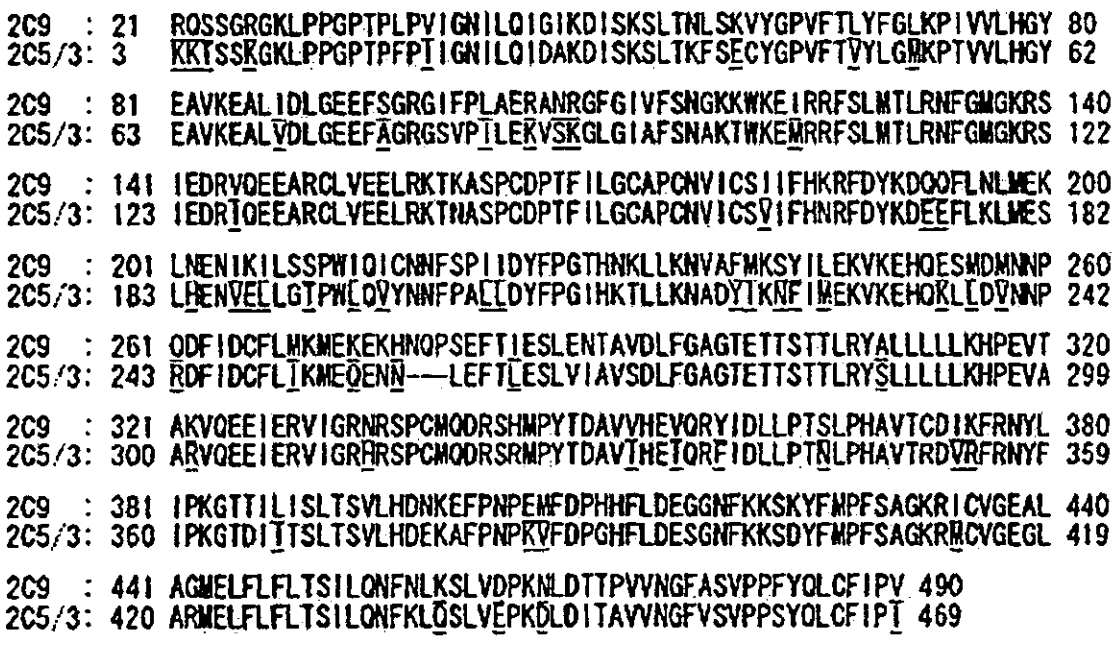

(b) CYP2C9

Fig. 2. Sequence alignments of CYP2C19 and CYP2C9 against CYP2C5/3LVdH. The identical residues were expressed by meshed letters and the underlined residues were positives.

the ligand (S)-mephenytoin was surrounded by hydrophobic amino acids such as Val113, Ile205, Ala297 and Phe476, which were conserved in all wild types and mutants in this study. Furthermore, proteins for which the solutions of CScore = 5 were not obtained by computational docking trials based on the hydrogen-bond query from carbonyl oxygen of Asp293 (that is, CYP2C19.5A and CYP2C19.5B) were experimentally inactive mutants.

Table III. Identities and Positives[a] Between Amino-Acid Sequences of CYP2Cs

	CYP2C5/3LVdH	CYP2C19	CYP2C9
CYP2C5/3LVdH	100%	75%	75%
CYP2C19	87%	100%	92%
CYP2C9	87%	96%	100%

[a] Identities and positives were described in upper right and lower left portions, respectively.

By contrast, for the experimentally inactive protein 2, docking models with CScore values of 5 were also obtained. Thus, we carried out more structure refinement for ligand-free protein 2 using MD simulation, steepest-descent and conjugate-gradient optimizers. After the refinement, we also performed additional computational docking for the refined structure with (S)-mephenytoin. Figure 7 shows the three-dimensional structures of protein 2 before and after the refinement. This reveals that structural features, such as the position of heme and the shape of the ligand-binding pocket around Asp293, were changed by MD calculations. After the structure refinement, no solutions of the docking trials of (S)-mephenytoin with protein 2 were obtained under the assumption that the hydrogen bond between carbonyl oxygen of Asp293 and (S)-mephenytoin are indispensable to ligand docking.

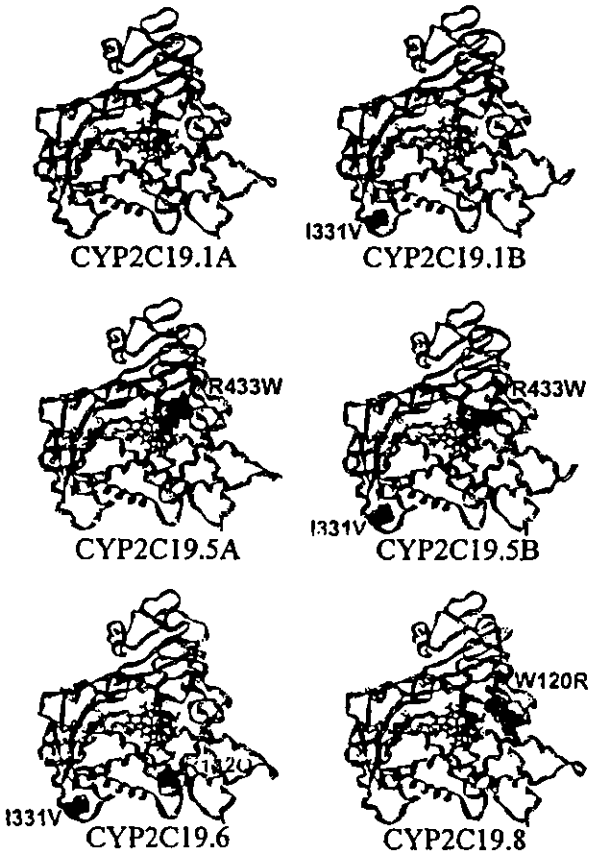

Fig. 3. Homology model for wild types and mutants of CYP2C19.

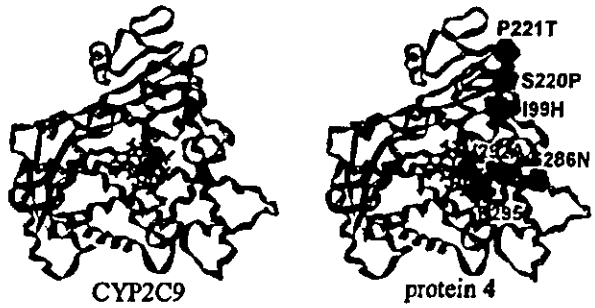

Fig. 4. Homology model for wild types and mutants of CYP2C9.

DISCUSSION

Homology models illustrated in Figs. 3 and 4 suggest that even if the mutated portions are not near the active sites (i.e., in adjacent regions of heme) mutations of one or two residues are still capable of inactivating CYP2C19. For example, Ile331Val, which does not affect the enzyme activity in CYP2C19.1B, and also mutations that play important roles for inactivities of mutants of CYP2C19 (Arg132Gln in CYP2C19.6), were positioned far from the ligand-binding pocket. Furthermore, although Arg433Trp in both CYP2C19.5A and CYP2C19.5B is located near by heme moiety, this residue is far away from the iron atom and does not seem to be directly implicated in the ligand docking. This indicates that mutations change the conformations of ligand-binding pockets of proteins, and affect the enzyme activities even if the mutations are located far from the ligand-binding pocket. By contrast, Ile99His, Ser286Asn, Val292Ala and Phe295Leu in protein 4 existed near the active site in our homology model. In particular, Ser286Asn, Val292Ala and Phe295Leu belong to the helix I, and these positions are also members of the substrate-recognition site 4 (SRS-4) (37). Therefore, these mutations might be directly implicated in (S)-mephenytoin docking for protein 4.

In the model of CYP2C19.1A complex with (S)-

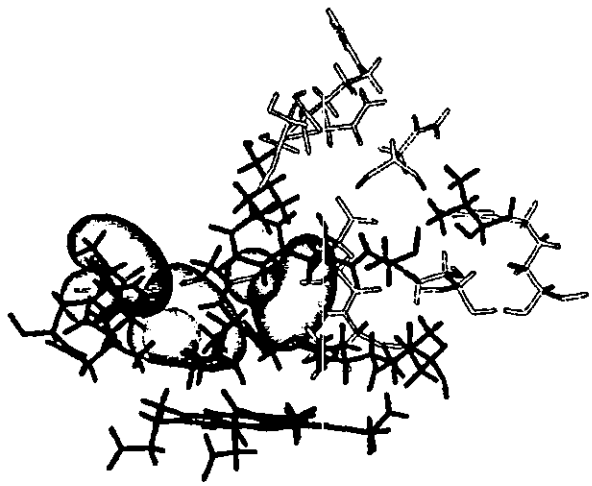

Fig. 5. Active-site residues explored by Site ID and hydrogen-bond queries in CYP2C19.1A. Hydrophobic amino acids are colored green; Asp293 and Gly296 are illustrated in red. Three hydrogen-bond queries were described with spatial constraint.

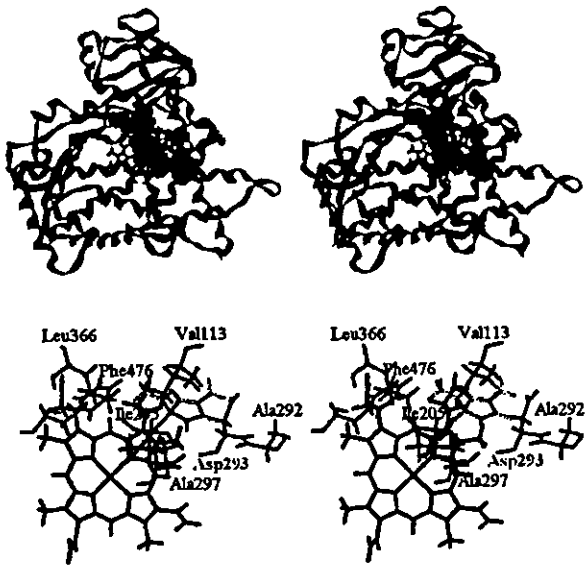

Fig. 6. CYP2C19.1A complex with (S)-mephenytoin. (S)-Mephenytoin, Asp293, and hydrophobic amino acids were illustrated in yellow, red, and green, respectively.

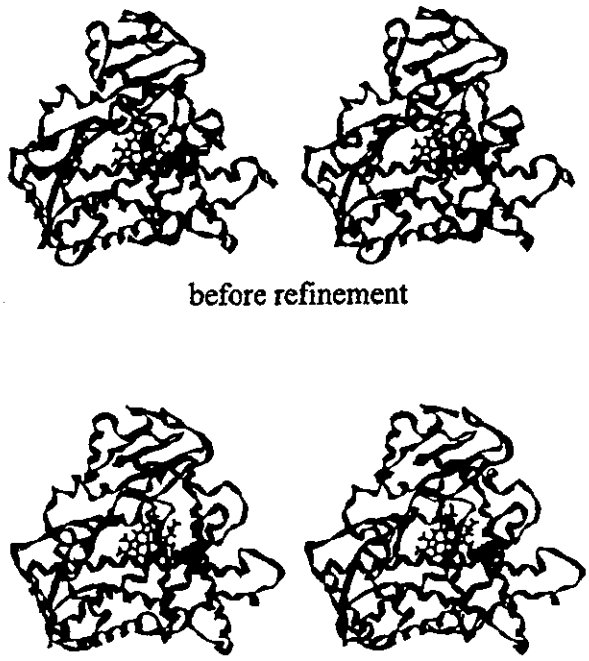

Fig. 7. Three-dimensional structures of protein 2 before and after refinement by MD simulation, steepest-decent and conjugate-gradient optimizers. The two structures were aligned by the fitting of their main chains. The RMSD of the protein 2 structure before and after refinement was 3.524 Å. The red colored residue was Asp293.

mephenytoin shown in Fig. 6, the orientation of (S)-mephenytoin whose 4′-hydrogen was located near the heme iron is consistent with (S)-mephenytoin 4′-hydroxylase activity of CYP2C19.1A and suggests that the three-dimensional structure of the calculated docking model is reasonable. The result that (S)-mephenytoin was surrounded by hydrophobic amino acids indicates that this hydrophobicity plays an important role for (S)-mephenytoin docking in the binding pocket of CYP2C19.1A. Significantly, Ala297 and Phe476 were located nearby the phenyl ring of ligand, suggesting that the CH-π interaction between the phenyl ring and Ala297, and/or the π-π stacking between ligand and Phe476, are important for the location of (S)-mephenytoin in CYP2C19.1A. Furthermore, Asp293 and Ala297, which seem to be important residues for ligand docking, are members of helix I and SRS-4. This is consistent with the results of Tsao *et al.* (11)

Table IV. The Results of Computational Docking

Protein	Experimental 4′-hydroxylase activity	Hydrogen bond query on Asp293[a]	Maximum CScore value[b]
2C19.1A	Active	OK	5
2C19.1B	Active	OK	5
2C19.5A	Inactive	OK	3
2C19.5B	Inactive	OK	4
2C19.6	Inactive	Bump	—
2C19.8	Active (*in vitro*)	OK	5
2C9	Inactive	Bump	—
1	Inactive	Bump	—
2	Inactive	OK	5
3	Inactive	Bump	—
4	Active	OK	5

[a] The result of VDW bump checks for hydrogen-bond query on Asp293.
[b] The best CScore value of those for all docking models.

For other proteins than CYP2C19.1A, hydrogen-bond queries constructed from the carbonyl oxygen of Asp293 in CYP2C19.6, CYP2C9, proteins 1 and 3 were omitted by the VDW bump check, and there were no docking models whose CScore values were 5 in CYP2C19.5A and CYP2C19.5B. For the refined model of protein 2, no solutions were obtained by the computational docking. Because all these proteins were experimentally observed enzyme inactivities without exceptions, these results support that Asp293 plays an important role in CYP2C19–(S)-mephenytoin complex. Furthermore, for CYP2C19.1B, CYP2C19.8 and proteins 4 computational docking calculations gave the solutions of CScore = 5, and these proteins were experimentally active. These results suggest that our methods applied to this study are reasonable for binding mode predictions.

Only recently, the three-dimensional structures of CYP2C5 complex with sulfaphenazole (38), ligand-free CYP2C9 and CYP2C9 complexed with warfarin (39), were determined by X-ray crystallographic analyses. Because the sizes of the ligands in these complexes were different from (S)-mephenytoin, these structures were not able to give critical clues for the investigation of the complex structure of CYP2C19 with (S)-mephenytoin. Furthermore, for the observed structure of the CYP2C9 complex with warfarin, the ligand molecule was not located in the usual position of CYP substrate-binding pockets. Although this is useful for investigating the mechanisms of inhibitions and allosteric effects of CYPs, it does not aid research into the binding modes of normal CYP substrates, such as (S)-mephenytoin. Nonethe-

less, when these data are used together with the results of computational docking studies in this paper, it might give some support to the predictions of complex structures. Comparing the structures of CYP2C19.1A with (S)-mephenytoin in this study, and CYP2C5 with sulfaphenazole in crystallographic data, it was found that Asp290 of CYP2C5 (the residue corresponding to Asp293 in CYP2C19.1A) was in the substrate-binding pocket and interacted with the ligand sulfaphenazole. This indicates that both Asp290 of CYP2C5 and Asp293 of CYP2C19.1A play significant roles in binding of substrates, and supports the validity of our model structure of CYP2C19 complex with (S)-mephenytoin.

CONCLUSIONS

In this study, we found that models produced by homology modeling and computational docking procedures of CYP complexed with (S)-mephenytoin were obtained for experimentally active enzymes but not for inactive proteins. The binding modes of all active enzymes were similar to wild-type CYP2C19.1A. For inactive proteins, hydrogen bonds between the carbonyl oxygen in the main chain of Asp293 and the ligand were not able to form, or the scores of the resulting docking models were low. These results indicate that the computational methods used in this study are useful for the investigation of the structures of ligand–protein complexes. Although more detailed confirmations of the importance of Asp293 for (S)-mephenytoin binding into CYP2C19 by using structural biologic methods such as X-ray diffraction or NMR spectroscopy were preferable, the role of Asp293 was supported by the results that all calculations for wild types and mutants are consistent with experimentally observed enzyme activities without exception.

Three-dimensional structures of biopolymers are very important for the rational drug design. Though the determinations of structures by experimental methods (i.e., X-ray diffraction or NMR) give the useful information for drug design, these experiments are expensive and time-consuming. Therefore, it is preferable that the three-dimensional structures of structurally unknown proteins were computationally predicted using known structures of homologous proteins. Especially, when many complexes have to be considered for drug design (i.e., the situation that there are many mutants such as CYP2C19), homology modeling play an important role in drug design studies because all structures can not be determined by experiments within reasonable costs. In this study, even if the mutated parts of the mutants were far from the substrate-binding pockets, such as CYP2C19.6, the computational results were consistent with the experimental activities. This suggests that the computational methods used in this study, especially for FAMS, are promising not only for wild-type enzymes but also for mutants. We expect that virtual screening trials can be carried out for several proteins using these methods.

REFERENCES

1. M. Romkes, M. B. Faletto, J. A. Blaisdell, J. L. Raucy, and J. A. Goldstein. Cloning and expression of complementary DNAs for multiple members of the human cytochrome P450IIC subfamily. *Biochemistry* 30:3247–3255 (1991).
2. S. A. Wrighton, J. C. Stevens, G. W. Becker, and M. VandenBranden. Isolation and characterization of human liver cytochrome P450 2C19: correlation between 2C19 and S-mephenytoin 4′-hydroxylation. *Arch. Biochem. Biophys.* 306: 240–245 (1993).
3. J. A. Goldstein, M. B. Faletto, M. Romkes-Sparks, T. Sullivan, S. Kitareewan, J. L. Raucy, J. M. Lasker, and B. I. Ghanayem. Evidence that CYP2C19 is the major (S)-mephenytoin 4′-hydroxylase in humans. *Biochemistry* 33:1743–1752 (1994).
4. A. Küpfer, P. Desmond, R. Patwardhan, S. Schenker, and R. A. Branch. Mephenytoin hydroxylation deficiency: kinetics after repeated doses. *Clin. Pharmacol. Ther.* 35:33–39 (1984).
5. S. M. F. de Morais, G. R. Wilkinson, J. Blaisdell, K. Nakamura, U. A. Meyer, and J. A. Goldstein. The major genetic defect responsible for the polymorphism of S-mephenytoin in humans. *J. Biol. Chem.* 269:15419–15422 (1994).
6. S. M. F. de Morais, G. R. Wilkinson, J. Blaisdell, K. Nakamura, U. A. Meyer, and J. A. Goldstein. Identification of a new genetic defect responsible for the polymorphism of S-mephenytoin metabolism in Japanese. *Mol. Pharmacol.* 46:594–598 (1994).
7. Z. S. Xiao, J. A. Goldstein, H.-G. Xie, J. Blaisdell, W. Wang, C.-H. Jiang, F.-X. Yan, N. He, S.-L. Huang, Z.-H. Xu, and H.-H. Zhou. Differences in the incidence of the CYP2C19 polymorphism affecting the S-mephenytoin phenotype in Chinese Han and Bai populations and identification of a new rare *CYP2C19* mutant allele. *J. Pharmacol. Exp. Ther.* 281:604–609 (1997).
8. R. J. Ferguson, S. M. F. de Morais, S. Benhamou, C. Bouchardy, J. Blaisdell, G. Ibeanu, G. R. Wilkinson, T. C. Sarich, J. M. Wright, P. Dayer, and J. A. Goldstein. A novel defect in human *CYP2C19*: mutation of the initiation codon is responsible for poor metabolism of S-mephenytoin. *J. Pharmacol. Exp. Ther.* 284:356–361 (1998).
9. G. C. Ibeanu, J. A. Goldstein, U. Meyer, S. Benhamou, C. Bouchardy, P. Dayer, and B. I. Ghanayem. and J. Blaisdell. Identification of new human *CYP2C19* alleles (*CYP2C19*6* and *CYP2C19*2B*) in a Caucasian poor metabolizer of mephenytoin. *J. Pharmacol. Exp. Ther.* 286:1490–1495 (1998).
10. G. C. Ibeanu, J. Blaisdell, B. I. Ghanayem, C. Beyeler, S. Benhamou, C. Bouchardy, G. R. Wilkinson, P. Dayer, A. K. Daly, and J. A. Goldstein. An additional defective allele, *CYP2C19*5*, contributes to the S-mephenytoin poor metabolizer phenotype in Caucasians. *Pharmacogenetics* 8:129–135 (1998).
11. G. C. Ibeanu, J. Blaisdell, R. J. Gerguson, B. I. Ghanayem, K. Brosen, S. Benhamou, C. Bouchardy, G. R. Wilkinson, P. Dayer, and J. A. Goldstein. A novel transversion in the intron 5 donor splice junction of *CYP2C19* and a sequence polymorphism in exon 3 contribute to the poor metabolizer phenotype for the anticonvulsant drug S-mephenytoin. *J. Pharmacol. Exp. Ther.* 290:635–640 (1999).
12. S. Kimura, J. Pastewka, H. V. Gelboin, and F. J. Gonzalez. cDNA and amino acid sequences of two members of the human P450IIC gene subfamily. *Nucleic Acids Res.* 15:10053–10054 (1987).
13. C.-C. Tsao, M. R. Wester, B. Ghanayem, S. J. Coulter, B. Chanas, E. F. Johnson, and J. A. Goldstein. Identification of human CYP2C19 residues that confer S-mephenytoin 4′-hydroxylation activity to CYP2C9. *Biochemistry* 40:1937–1944 (2001).
14. P. A. Williams, J. Cosme, V. Sridhar, E. F. Johnson, and D. E. McRee. Mammalian microsomal cytochrome P450 monooxygenase: structural adaptations for membrane binding and functional diversity. *Mol. Cell* 5:121–131 (2000).
15. R. D. Taylor, P. J. Jewsbury, and J. W. Essex. A review of protein-small molecule docking methods. *J. Comput. Aided Mol. Des.* 16:151–166 (2002).
16. M. Rarey, B. Kramer, T. Lengauer, and G. Klebe. A fast flexible docking method using an incremental construction algorithm. *J. Mol. Biol.* 261:470–489 (1996).
17. T. J. Ewing. DOCK 4.0: search strategies for automated molecular docking of flexible molecule databases. *J. Comput. Aided Mol. Des.* 15:411–428 (2001).
18. G. Jones, P. Willet, R. C. Glen, A. R. Leach, and R. Taylor. Development and validation of a genetic algorithm for flexible docking. *J. Mol. Biol.* 267:727–748 (1997).
19. D. F. V. Lewis, M. Dickins, R. J. Weaver, P. J. Eddershaw, P. S. Goldfarb, and M. H. Tarbit. Molecular modeling of human CYP2C subfamily enzymes CYP2C9 and CYP2C19: rationalization of substrate specificity and site-directed mutagenesis experiments in the CYP2C subfamily. *Xenobiotica* 28:235–268 (1998).
20. V. A. Payne, Y.-T. Chang, and G. H. Loew. Homology modeling

and substrate binding study of human CYP2C18 and CYP2C19 enzymes. *Proteins* 37:204–217 (1999).
21. M. Ridderström, I. Zamora, O. Fjellström, and T. B. Andersson. Analysis of selective regions in the active sites of human cytochromes P450, 2C8, 2C9, 2C18 and 2C19 homology models using GRID/CPCA. *J. Med. Chem.* 44:4072–4081 (2001).
22. D. F. V. Lewis. Modeling human cytochromes P450 involved in drug metabolism from the CYP2C5 crystallographic template. *J. Inorg. Biochem.* 91:502–514 (2002).
23. M. J. de Groot, A. A. Alex, and B. C. Jones. Development of a combined protein and pharmacophore model for cytochrome P450 2C9. *J. Med. Chem.* 45:1983–1993 (2002).
24. K. Ogata and H. Umeyama. An automatic homology modeling method consisting of database searches and simulated annealing. *J. Mol. Graphics Mod.* 18:258–272 (2000).
25. D. A. Case, D. A. Pearlman, J. W. Caldwell, T. E. Cheatham, W. S. Ross, C. Simmerling, Y. Duan, J. Pitera, I. Massova, G. L. Seibel, U. C. Singh, P. Weiner, and P. A. Kollman. *AMBER 6*, University of California, San Francisco, CA 1999.
26. U. C. Singh and P. A. Kollman. An approach to computing electrostatic charges for molecules. *J. Comput. Chem.* 5:129–145 (1984).
27. M. J. Frisch, G. W. Trucks, H. B. Schlegel, G. E. Scuseria, M. A. Robb, J. R. Cheeseman, V. G. Zakrzewski, J. A. Montgomery, R. E. Stratmann, J. C. Burant, S. Dapprich, J. M. Millam, A. D. Daniels, K. N. Kudin, M. C. Strain, O. Farkas, J. Tomasi, V. Barone, M. Cossi, R. Cammi, B. Mennucci, C. Pomelli, C. Adamo, S. Clifford, J. Ochterski, G. A. Petersson, P. Y. Ayala, Q. Cui, K. Morokuma, D. K. Malick, A. D. Rabuck, K. Raghavachari, J. B. Foresman, J. Cioslowski, J. V. Ortiz, A. G. Baboul, B. B. Stefanov, G. Liu, A. Liashenko, P. Piskorz, I. Komaromi, R. Gomperts, R. L. Martin, D. J. Fox, T. Keith, M. A. Al-Laham, C. Y. Peng, A. Nanayakkara, C. Gonzalez, M. Challacombe, P. M. W. Gill, B. G. Johnson, W. Chen, M. W. Wong, J. L. Andres, M. Head-Gordon, E. S. Replogle, and J. A. Pople. *Gaussian 98 Revision A.7*, Gaussian, Inc, Wallingford, CT 1998.
28. H. Tsujishita and S. Hirono. CAMDAS: an automated conformational analysis system using molecular dynamics. *J. Comput. Aided Mol. Des.* 11:305–315 (1997).
29. T. A. Halgren. Merck molecular force field. I. Basis, form, scope, parameterization, and performance of MMFF94. *J. Comput. Chem.* 17:490–519 (1996).
30. I. Muegge and Y. C. Martin. A general and fast scoring function for protein–ligand interactions: a simplified potential approach. *J. Med. Chem.* 42:791–804 (1999).
31. I. D. Kuntz, J. M. Blaney, S. J. Oatley, R. Langridge, and T. E. Ferrin. A geometric approach to macromolecule–ligand interactions. *J. Mol. Biol.* 161:269–288 (1982).
32. M. D. Eldridge, C. W. Murray, T. R. Auton, G. V. Paolini, and R. P. Mee. Empirical scoring functions: I. The development of a fast empirical scoring function to estimate the binding affinity of ligands in receptor complexes. *J. Comput. Aided Mol. Des.* 11: 425–445 (1997).
33. P. S. Charifson, J. J. Corkery, M. A. Murcko, and W. P. Walters. Consensus scoring: a method for obtaining improved hit rates from docking databases of three-dimensional structures into proteins. *J. Med. Chem.* 42:5100–5109 (1999).
34. R. D. Clark, A. Strizhev, J. M. Leonard, J. F. Blake, and J. B. Matthew. Consensus scoring for ligand/protein interactions. *J. Mol. Graphics Mod* 20:281–295 (2002).
35. W. L. Jorgensen, J. Chandrasekhar, J. D. Madura, R. W. Impey, and M. L. Klein. Comparison of simple potential functions for simulating liquid water. *J. Chem. Phys.* 79:926–935 (1983).
36. J. P. Ryckaert, G. Cicotti, and H. J. C. Berensden. Numerical integration of the Cartesian equations of motion of a system with constraints: molecular dynamics of *n*-alkanes. *J. Comput. Phys.* 23:327–341 (1977).
37. O. Gotoh. Substrate recognition sites in cytochrome P450 family 2 (CYP2) proteins inferred from comparative analyses of amino acid and coding nucleotide sequences. *J. Biol. Chem.* 267:83–90 (1992).
38. M. R. Wester, E. F. Johnson, C. Marques-Soares, P. M. Dansette, D. Mansuy, and C. D. Stout. Structure of a substrate complex of mammalian cytochrome P450 2C5 at 2.3 Å resolution: evidence for multiple substrate binding modes. *Biochemistry* 42:6370–6379 (2003).
39. P. A. Williams, J. Cosme, A. Ward, H. C. Angove, D. M. Vinkovi, and H. Jhoti. Crystal structure of human cytochrome P450 2C9 with bound warfarin. *Nature* 424:464–468 (2003).

0090-9556/04/3209-1040–1047$20.00
DRUG METABOLISM AND DISPOSITION
Copyright © 2004 by The American Society for Pharmacology and Experimental Therapeutics
DMD 32:1040–1047, 2004

Vol. 32, No. 9
1417/1169877
Printed in U.S.A.

CARRIER-MEDIATED UPTAKE OF H_2-RECEPTOR ANTAGONISTS BY THE RAT CHOROID PLEXUS: INVOLVEMENT OF RAT ORGANIC ANION TRANSPORTER 3

Yoshinori Nagata, Hiroyuki Kusuhara, Shuichi Hirono, Hitoshi Endou, and Yuichi Sugiyama

Graduate School of Pharmaceutical Sciences, the University of Tokyo, Hongo, Bunkyo-ku, Tokyo, Japan (Y.N., H.K., Y.S.); School of Pharmaceutical Sciences, Kitasato University, Shirokane, Mitano-ku, Tokyo, Japan (S.H.); and Department of Pharmacology and Toxicology, Kyorin University School of Medicine, Shinkawa, Mitaka, Tokyo, Japan (H.E.)

Received February 17, 2004; accepted May 20, 2004

This article is available online at http://dmd.aspetjournals.org

ABSTRACT:

The choroid plexus (CP) acts as a site for the elimination of xenobiotic organic compounds from the cerebrospinal fluid (CSF). The purpose of the present study is to investigate the role of rat organic anion transporter 3 (rOat3; *Slc22a8*) in the uptake of H_2-receptor antagonists (cimetidine, ranitidine, and famotidine) by the isolated rat CP. Saturable uptake of cimetidine and ranitidine was observed in rOat3-LLC with K_m values of 80 and 120 μM, respectively, whereas famotidine was found to be a poor substrate. The steady-state concentration of the H_2-receptor antagonists in the CSF was significantly increased by simultaneously administered probenecid, although it did not affect their brain and plasma concentrations. Saturable uptake of cimetidine and ranitidine was observed in the isolated rat CP with K_m values of 93 and 170 μM, respectively, whereas 50% of the uptake of famotidine remained at the highest concentration examined (1 mM). The K_i value of ranitidine for the uptake of cimetidine by the isolated CP (50 μM) was similar to its own K_m value, suggesting that they share the same transporter for their uptake. The inhibition potency of organic anions such as benzylpenicillin, estradiol 17β-glucuronide, *p*-aminohippurate, and estrone sulfate for the uptake of cimetidine by the isolated rat CP was similar to that for benzylpenicillin, the uptake of which has been hypothesized to be mediated by rOat3, whereas a minimal effect by tetraethylammonium excludes involvement of organic cation transporter(s). These results suggest that rOat3 is the most likely candidate transporter involved in regulating the CSF concentration of H_2-receptor antagonists at the CP.

The choroid plexus (CP), located in the lateral, third, and fourth ventricles, is the site of production of cerebrospinal fluid (CSF) (Segal, 2000; Haselbach et al., 2001). It is well established that CP acts as a barrier between the CSF and the circulating blood, and it is referred to as the blood-CSF barrier (Suzuki et al., 1997; Ghersi-Egea and Strazielle, 2001; Haselbach et al., 2001; Kusuhara and Sugiyama, 2001). The barrier function is achieved partly by the tight monolayer of choroid plexus epithelial cells and partly by detoxification systems consisting of metabolic enzymes and multispecific transporters (Suzuki et al., 1997; Ghersi-Egea and Strazielle, 2001; Haselbach et al., 2001; Kusuhara and Sugiyama, 2001).

Histamine H_2-receptor antagonists have been used clinically to cure duodenal ulcers and gastric acid hypersecretion, and adverse effects by H_2-receptor antagonists on the central nervous system, ranging from mild dizziness, restlessness, and mental confusion to advanced symptoms such as myoclonic twitching and seizure, have been reported (Grimson, 1977; Schentag et al., 1979; McGuigan, 1981). Schentag et al. (1979) reported that the concentration of cimetidine in the CSF is related to the mental status. We demonstrated previously that a saturable mechanism is involved in the elimination of cimetidine from the CSF after intracerebroventricular administration (Suzuki et al., 1985, 1988). Transport studies revealed that the uptake of cimetidine by the isolated rat choroid plexus is saturable, and the efflux transport across the CP has been considered to account for the saturable elimination mechanism of cimetidine from the CSF (Suzuki et al., 1986). Organic anions such as benzylpenicillin and *p*-aminohippurate (PAH) inhibit the uptake of cimetidine by the isolated rat choroid plexus, whereas organic cations such as tetraethylammonium (TEA) and *N*-methylnicotinamide have no such effect (Suzuki et al., 1986). It is likely that organic anion transporter(s) play a major role in regulating the CSF concentration of cimetidine at the CP.

We have isolated rat organic anion transporter 3 (rOat3; *Slc22a8*), the third isoform of the Oat/OAT family, from the rat brain cDNA library by homology cloning (Kusuhara et al., 1999). Functional expression of rOat3 in *Xenopus laevis* oocytes and mammalian cells has revealed its broad substrate specificity for organic anions, including PAH and benzylpenicillin (Kusuhara et al., 1999; Burckhardt and Burckhardt, 2003; Dantzler and Wright, 2003). In the CP, although mRNA expression of all the Oat isoforms (rOat1–rOat3) has been detected (Sweet et al., 2002; Choudhuri et al., 2003), rOat3 is the most abundant isoform (Choudhuri et al., 2003). rOat3 has been shown to be expressed on the brush border membrane of the CP (Nagata et al., 2002). Localization of rOat3 in the CP suggests its involvement in the uptake process at the CP. Since the spectrum of inhibitors and kinetic

This work was supported by grant-in-aids from the Ministry of Health, Labor and Welfare of Japan and a grant-in-aid for Scientific Research (B) (KAKENHI 15390035).

ABBREVIATIONS: CP, choroid plexus; CSF, cerebrospinal fluid; PAH, *p*-aminohippurate; TEA, tetraethylammonium; Oat, organic anion transporter; MEP, molecular electrostatic potential(s); LC-MS, liquid chromatography-mass spectometry; Oct, organic cation transporter.

parameters for the uptake of PAH and benzylpenicillin by the isolated rat CP were similar to those for rOat3, it has been hypothesized that rOat3 accounts for their uptake by the isolated rat CP (Nagata et al., 2002). Furthermore, the finding that the isolated choroid plexus from mOat3 knockout mice was unable to cellularly accumulate fluorescein supports the role of Oat3 in the CP (Sweet et al., 2002). H_2-receptor antagonists have been referred to as bisubstrates recognized by both renal organic anion and cation transporters (Ullrich et al., 1993). Indeed, cimetidine is a substrate of rOat3 as well as organic cation transporter(s) (Grundemann et al., 1999; Kusuhara et al., 1999). Therefore, it is likely that rOat3 plays a major role in the uptake of cimetidine and other H_2-receptor antagonists by the isolated rat CP.

The primary purpose of the present study was to investigate the importance of rOat3 in regulating the concentration of H_2-receptor antagonists (cimetidine, ranitidine, and famotidine). We examined whether ranitidine and famotidine are substrates of rOat3 in LLC-PK1 cells expressing rOat3 (rOat3-LLC). rOat3-LLC exhibits specific uptake of ranitidine and famotidine, but the transport activity of famotidine was quite low compared with that of cimetidine and ranitidine. Steady-state concentrations of H_2-receptor antagonists in the CSF and plasma were determined in rats treated with or without probenecid, a potent inhibitor of rOat3. The uptake of H_2-receptor antagonists was investigated using the isolated rat CP, and the kinetic parameters and spectrum of inhibitors were compared with those for benzylpenicillin.

Materials and Methods

Materials. [^{3}H]Cimetidine (16.5 Ci/mmol) and [^{14}C]urea (52 mCi/mmol) were purchased from Amersham Biosciences UK, Ltd. (Little Chalfont, Buckinghamshire, UK). All cell culture media and reagents were obtained from Invitrogen (Carlsbad, CA), except fetal bovine serum (Cansera International Inc., Ontario, Canada). All other chemicals and reagents were of analytical grade and readily available from commercial sources.

Calculation of Molecular Electrostatic Potential (MEP) of H_2-Receptor Antagonists. The starting structures of H_2-receptor antagonists were built up on the basis of standard bond lengths and angles, and the structures of H_2-receptor antagonists were optimized using the AM1 Hamiltonian and conductor-like screening model. Their molecular electrostatic potentials at pH 7.4 were calculated using the modified neglect of diatomic overlap Hamiltonian. All calculations were carried out by the MOPAC97 (CS Chem3D Pro; CambridgeSoft Corporation, Cambridge, MA).

Uptake Studies by rOat3-LLC. rOat3-LLC was established previously, and all the procedures have been described in detail (Sugiyama et al., 2001). Cells were seeded on a 12-well dish (BD Biosciences, Franklin Lakes, NJ) at a density of 1.2×10^5 cells/well and cultured for 3 days. Sodium butyrate (5 mM) was added to the culture medium to induce expression of the transporter 24 h before starting the experiments (Sugiyama et al., 2001). Uptake was initiated by adding medium containing ligands, with or without inhibitors, after the cells had been washed twice and preincubated with Krebs-Henseleit buffer at 37°C for 15 min. This buffer consists of 142 mM NaCl, 23.8 mM Na_2CO_3, 4.83 mM KCl, 0.96 mM KH_2PO_4, 1.20 mM $MgSO_4$, 12.5 mM HEPES, 5 mM glucose, and 1.53 mM $CaCl_2$ adjusted to pH 7.4. The uptake was terminated at a designated time by adding ice-cold Krebs-Henseleit buffer. For [^{3}H]cimetidine uptake, cells were dissolved in 500 μl of 1 N NaOH, kept overnight, neutralized with 250 μl of 2 N HCl, and then aliquots (500 μl) were transferred to scintillation vials. The radioactivity associated with the cells and medium was determined in a liquid scintillation spectrophotometer (LS6000SE; Beckman Coulter, Fullerton, CA) after adding scintillation fluid (Hionic-Fluor; PerkinElmer Life and Analytical Sciences, Boston, MA) to the vials. For the determination of the uptake of ranitidine and famotidine, cells were dissolved in 200 μl of 0.2 N NaOH, and aliquots (50 μl) were used for LC-MS quantification as described below. The remaining portions of cell lysate were used to determine the protein concentration by the method of Lowry, with bovine serum albumin as a standard. Ligand uptake was given as the cell-to-medium concentration ratio determined as the amount of ligand associated with cells divided by the medium concentration.

Uptake Studies by Isolated Rat CP. Male Sprague-Dawley rats weighing 250 to 300g were purchased from SLC (Shizuoka, Japan). The CP was isolated from the lateral ventricles and incubated at 37°C for 1 min in 500 μl of artificial CSF, which consists of 122 mM NaCl, 25 mM $NaHCO_3$, 10 mM glucose, 3 mM KCl, 1.4 mM $CaCl_2$, 1.2 mM $MgSO_4$, 0.4 mM K_2HPO_4, and 10 mM HEPES (pH 7.3), equilibrated with 95% O_2/5% CO_2. Radiolabeled ligands, with or without inhibitors, were added simultaneously to initiate uptake. The uptake of [^{3}H]cimetidine and [^{14}C]TEA by isolated rat CP was examined by centrifugal filtration as described previously (Nagata et al., 2002). The tissue-to-medium concentration ratio of [^{3}H]cimetidine and [^{14}C]TEA was calculated with [^{14}C]urea or [^{3}H]water as a cell water space marker and corrected for the adherent water space. The ^{3}H and ^{14}C activity in the specimens was determined in a liquid scintillation spectrophotometer. To determine the uptake of nonradiolabeled H_2-receptor antagonists, the rapid filtration method was used since the silicon oil, used in the centrifugal filtration method, disturbed the quantification by LC-MS. The uptake of cimetidine, ranitidine, and famotidine by isolated rat CP was terminated by rapid filtration using a vacuum manifold; then the CP was rinsed three times with 300 μl of artificial CSF, the CP was dissolved in 100 μl of 0.2 N NaOH, and aliquots (50 μl) were subjected to LC-MS quantification as described below. The remaining portions of lysate were used to determine the protein concentration by the method of Lowry, with bovine serum albumin as a standard.

Constant Infusion Study In Rats. Rats were lightly anesthetized with ether, and the left femoral vein was cannulated with polyethylene tubing (PE-50; BD Biosciences). The priming dose of the H_2 antagonist and probenecid was 2 and 15 mg/kg, respectively. The H_2 antagonist and probenecid were given to rats through the femoral vein cannula at 2 and 30 mg/h/kg, respectively, for 3 h. The dose regimen was designed to obtain a CSF concentration of probenecid sufficient to inhibit rOat3. Blood samples (300 μl) were collected from the tail vein at 1 and 2 h during the infusion. At the end of the experiment, blood samples were collected from the abdominal vein, and animals were sacrificed by bleeding the abdominal aorta under ether anesthesia. Following sacrifice, 50- to 100-μl aliquots of CSF were obtained by cisternal puncture using insulin syringes (0.5-ml syringe with a 29-gauge × 1/2-inch attached needle; TERUMO Corporation, Tokyo, Japan), and whole brains were removed and weighed. To obtain plasma, blood was centrifuged at 10,000g for 5 min. For determination of the unbound plasma concentration, aliquots (0.5 ml) of plasma specimens were subjected to filtration (2500 rpm, 10 min) (MPS-1; Millipore Corporation, Bedford, MA). The brain samples were homogenized in three volumes of water using a Polytron homogenizer (Brinkmann Instruments, Westbury, NY). The concentrations of H_2-receptor antagonists and probenecid in plasma, plasma ultrafiltrate, and brain homogenate were quantified by LC-MS as described below.

Quantification of H_2-Receptor Antagonists and Probenecid by LC-MS. The quantification of cimetidine, ranitidine, famotidine, and probenecid was performed by a high-performance liquid chromatograph (Alliance 2690; Waters, Milford, MA) connected to a mass spectrometer (ZMD; Micromass UK Ltd., Manchester, UK). Aliquots (50 μl) of samples containing H_2-receptor antagonists were precipitated by adding 100 μl of methanol containing an internal standard (famotidine for cimetidine and ranitidine and cimetidine for famotidine), mixed, and centrifuged, and 20 μl of the supernatants was subjected to LC-MS. Aliquots (50 μl) of samples containing probenecid were precipitated by adding 100 μl methanol, mixed, and centrifuged, and aliquots (10 μl) of the supernatants were diluted with 990 μl of methanol, 20 μl of which was subjected to LC-MS. High-performance liquid chromatography analysis was performed on an Waters Xterra MS C18 column (2.5 μm, 3 mm i.d., 30 mm) at room temperature. Elution was performed with a 0 to 100% linear gradient of 10 mM ammonium acetate/methanol over 4 min at 0.8 ml/min. A portion of the eluent (split ratio = 1:3) was introduced into the MS via an electrospray interface. Detection was performed by selective ion monitoring in positive ion mode (m/z: 253, 315, 338, and 286 for cimetidine, ranitidine, famotidine, and probenecid, respectively).

Kinetic Analyses. Kinetic parameters were obtained using the Michaelis-Menten equation $v = V_{max} \times S/(K_m + S) + P_{dif} \times S$, where v is the uptake rate of the substrate (pmol/min/mg protein or pmol/min/μl tissue), S is the substrate concentration in the medium (μM), K_m is the Michaelis-Menten constant (μM), and V_{max} is the maximum uptake rate (pmol/min/mg protein or pmol/min/μl tissue). P_{dif} represents the uptake clearance corresponding to the

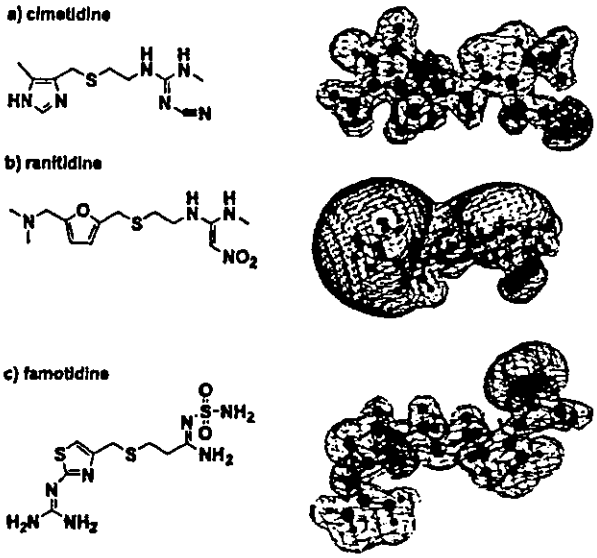

FIG. 1. Molecular structures and molecular electrostatic potential of H_2-receptor antagonists. MEP of cimetidine, ranitidine, and famotidine at pH 7.4 were calculated using the MNDO Hamiltonian. The figure illustrates the isoelectric line at 2.8 atomic units. The colors indicate the charge of their electrostatic potential: red is positive and blue is negative.

nonsaturable component (μl/min/mg protein or μl/min/μl tissue). To obtain the kinetic parameters, the equation was fitted to the uptake velocity using a MULTI program (Yamaoka et al., 1981). The input data were weighted as the reciprocals of the observed values, and the Damping Gauss-Newton method algorithm was used for fitting. Inhibition constants (K_i) were calculated by assuming competitive inhibition using the equation $CL_{+Inh} = CL/(1 + I/K_i) + P_{ns}$, where CL represents the uptake clearance and $_{+Inh}$ represents the value in the presence of inhibitor. I represents the concentration of inhibitor (μM). The substrate concentration was low compared with its K_m value in the inhibition study.

Results

Molecular Electrostatic Potential of H_2-Receptor Antagonists. Figure 1 illustrates the chemical structures of the H_2-receptor antagonists and their isoelectric lines at 2.8 atomic units calculated at pH 7.4. There was a region showing negative MEP in the chemical structures of H_2-receptor antagonists (Fig. 1; indicated by blue in the cyanoimine group for cimetidine, the nitro group for ranitidine, and the imine and sulfonamide groups for famotidine).

Uptake of H_2-Receptor Antagonists (Cimetidine, Ranitidine, and Famotidine) by rOat3-LLC. Figure 2 shows the time profiles of the uptake of cimetidine, ranitidine, and famotidine by vector- and rOat3-LLC. The uptake of cimetidine, ranitidine, and famotidine was significantly greater in rOat3-LLC than in vector-LLC, although the absolute value of famotidine uptake was quite small compared with that of cimetidine and ranitidine (Fig. 2). For further analyses, the uptake of cimetidine and ranitidine was determined at the earliest time, both technically and practically (3 min for cimetidine and 5 min for ranitidine). The uptake of cimetidine and ranitidine was saturable (Fig. 3), and kinetic analyses revealed that the K_m and V_{max} values of cimetidine and ranitidine by rOat3-LLC were 79.2 ± 17.8 and 121 ± 36 μM and 150 ± 29 and 367 ± 95 pmol/min/mg protein, respectively. The uptake clearance corresponding to the saturable component (V_{max}/K_m) for cimetidine and ranitidine was 1.89 ± 0.30 and 3.03 ± 0.39 μl/min/mg protein, respectively, whereas that corresponding to the nonsaturable component was 1.07 ± 0.03 and 0.381 ± 0.023 μl/min/mg protein, respectively.

Effect of Organic Anions and Cations on the Uptake of Cimetidine by rOat3. Benzylpenicillin and ranitidine inhibited the rOat3-mediated [^{3}H]cimetidine uptake in a concentration-dependent manner (Fig. 4, a and b), whereas TEA had no inhibitory effect at the concentrations examined (0.1 to 10 mM; data not shown). The K_i values of benzylpenicillin and ranitidine for cimetidine uptake by rOat3-LLC were determined to be 76.7 ± 13.2 and 119 ± 44 μM, respectively. Famotidine only weakly inhibited the uptake of cimetidine by rOat3-LLC (Fig. 4c).

Effect of Probenecid on the Plasma, Brain, and CSF Concentrations of H_2-Receptor Antagonists. Rats were given H_2-receptor antagonists by constant infusion with or without probenecid. The plasma concentrations of H_2-receptor antagonists reached steady-state within 3 h (data not shown), whereas the plasma concentration of probenecid showed a gradual increase during infusion (355 ± 107 μM at 1 h, 514 ± 143 μM at 2 h, and 651 ± 246 μM at 3h). The unbound plasma concentration and CSF concentration of probenecid at 3 h were 154 ± 26 and 57.3 ± 2.0 μM, respectively. Probenecid treatment did not affect the brain and plasma concentrations of the H_2-receptor antagonists (Table 1), whereas their CSF concentrations significantly increased (Table 1). The CSF-to-unbound plasma concentration ratio ($C_{CSF}/C_{p,fu}$) significantly increased by 3.7-fold for cimetidine, 4.3-fold for ranitidine, and 2.5-fold for famotidine (Table 1).

Uptake of H_2-Receptor Antagonists by the Isolated Rat CP. The time profiles of the uptake of [^{3}H]cimetidine and [^{14}C]TEA by isolated rat CP are shown in Fig. 5a (uptake units: μl/μl CP volume) and those of cimetidine, ranitidine, and famotidine are shown in Fig. 5b (uptake units: μl/mg protein). All the H_2-receptor antagonists showed time-dependent accumulation by the isolated rat CP, and their transport activities were in the following order: ranitidine ≈ cimetidine > famotidine (Fig. 5b). The uptake of TEA by the isolated rat CP was small compared with that of H_2-receptor antagonists (Fig. 5a). The uptake of [^{3}H]cimetidine and ranitidine was saturable, and kinetic analyses revealed that the uptake of [^{3}H]cimetidine and ranitidine consists of one saturable and one nonsaturable component (Fig. 6). The K_m and V_{max} values and uptake clearance corresponding to the nonsaturable component of [^{3}H]cimetidine were 92.7 ± 46.1 μM, 137 ± 71 pmol/min/μl tissue, and 0.581 ± 0.123 μl/min/μl tissue, respectively, whereas the corresponding values for ranitidine were 171 ± 57 μM, 1250 ± 360 pmol/min/mg protein, and 1.49 ± 0.26 μl/min/mg protein. The uptake of famotidine was saturated at high substrate concentrations (Table 2), but 50% of the total uptake remained at the highest concentration examined (1 mM, Table 2).

Effect of Organic Anions and TEA on the Uptake of Cimetidine by Isolated Rat CP. The effect of benzylpenicillin and TEA was examined with regard to the uptake of cimetidine, ranitidine, and famotidine by the isolated rat CP (Table 2). Benzylpenicillin inhibited the uptake of the H_2-receptor antagonists in a concentration-dependent manner. TEA did not affect the uptake of H_2-receptor antagonists. Furthermore, the effect of estradiol-17β-glucuronide, estrone sulfate, benzylpenicillin, PAH, ranitidine, and famotidine was also examined with regard to the uptake of [^{3}H]cimetidine by isolated rat CP (Fig. 7). All organic anions, ranitidine, and famotidine showed a concentration-dependent inhibition of the uptake of [^{3}H]cimetidine by the isolated rat CP (Fig. 7), and their inhibition constants are summarized in Table 3. The K_i and K_m values for the uptake of benzylpenicillin and cimetidine by the isolated rat CP were comparable (Table 3).

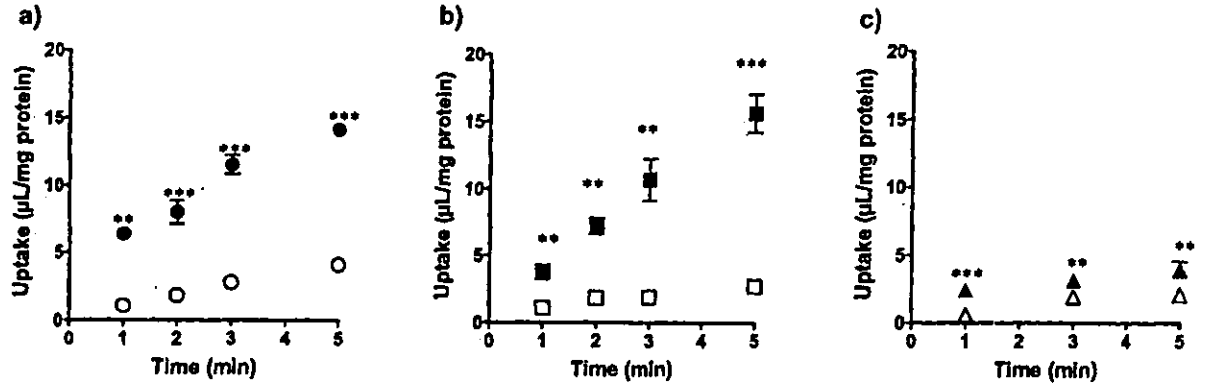

FIG. 2. Uptake of cimetidine, ranitidine, and famotidine by rOat3-LLC. The uptake of [^{3}H]cimetidine (a; circle), ranitidine (b; square) and famotidine (c; triangle) by rOat3-LLC (closed symbol) and vector-LLC (open symbol) was determined. The uptake was initiated by adding ligand ([^{3}H]cimetidine (1 μM), ranitidine (10 μM), and famotidine (10 μM) and terminated at designated times by adding ice-cold buffer. Each point represents the mean ± S.E. (n = 3–6). **, $p < 0.01$ and ***, $p < 0.001$, significantly different from vector-LLC (unpaired t test).

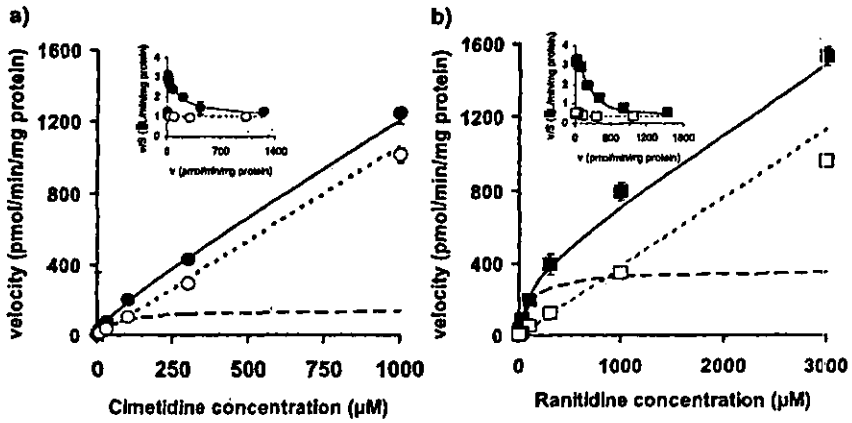

FIG. 3. Concentration dependence of the uptake of cimetidine and ranitidine by rOat3-LLC. The cellular accumulation of [^{3}H]cimetidine (a) and ranitidine (b) by rOat3-LLC for 3 and 5 min was determined at different substrate concentrations. The concentration dependence of the uptake of cimetidine and ranitidine by rOat3-LLC is shown as Eadie-Hofstee plots in the inset. Kinetic analyses revealed that the uptake of [^{3}H]cimetidine and ranitidine consists of one saturable and one nonsaturable component and follows the Michaelis-Menten equation. The solid, dotted, and broken lines represent the fitted line, the clearance of the nonsaturable component, and the clearance of the saturable component obtained by nonlinear regression analysis, respectively. Each point represents the mean ± S.E. (n = 3–6).

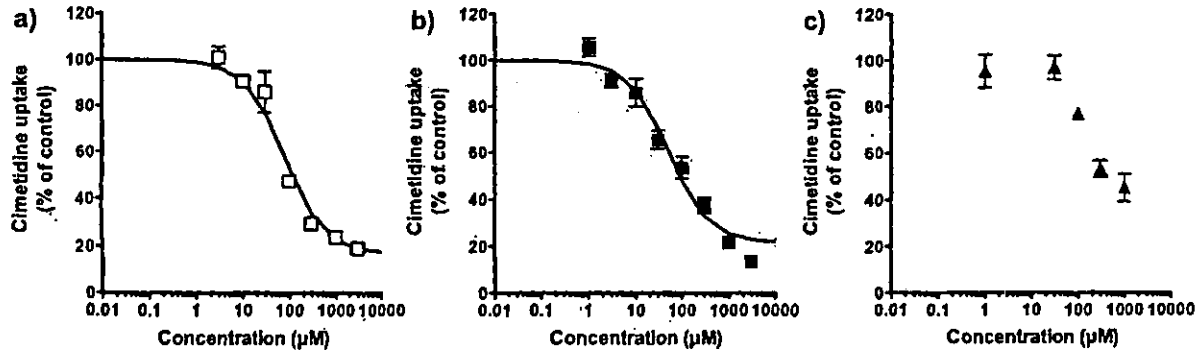

FIG. 4. Effect of organic anions and cations on the uptake of cimetidine by rOat3. The cellular accumulation of [^{3}H]cimetidine (1 μM) by rOat3 for 3 min was determined in the presence and absence of nonradiolabeled compounds at the concentrations indicated. Symbols represent benzylpenicillin (a; □), ranitidine (b; ■), and famotidine (c; ▲). The inhibition constants (K_i) of these compounds were calculated by assuming competitive inhibition. The solid lines represent the fitted line obtained by nonlinear regression analysis. The details of the fitting are described under *Materials and Methods*. Each point represents the mean ± S.E. (n = 3).

Discussion

In the present study, we reported that rOat3 is involved in the uptake of H_2-receptor antagonists (cimetidine, ranitidine, and famotidine) by the isolated rat CP, and that drug-drug interaction causes an increase in the CSF concentration of H_2-receptor antagonists without affecting their plasma concentration. rOat3 has been characterized by

TABLE 1

Total plasma, unbound plasma, CSF, and brain concentrations of H_2-receptor antagonists after intravenous infusion in rats treated with or without probenecid

H_2-receptor antagonists (2 mg/kg) were administered to rats by bolus intravenous administration followed by constant infusion (2 mg/h/kg) during 3 h. Probenecid (15 mg/kg) was administered to rats by bolus intravenous administration followed by constant infusion (30 mg/h/kg) during 3 h, and the unbound plasma concentrations and CSF concentrations of probenecid at 3 h were 154 ± 26 and 57.3 ± 2.0 μM, respectively. Each value represents the mean ± S.D. (n = 3).

	Cimetidine		Ranitidine		Famotidine	
	Control	+Probenecid	Control	+Probenecid	Control	+Probenecid
C_p (μM)	3.71 ± 1.20	2.97 ± 0.15	2.65 ± 1.25	2.11 ± 0.18	3.47 ± 1.22	2.79 ± 0.03
$C_{p,fu}$ (μM)	2.25 ± 0.60	1.89 ± 0.11	1.72 ± 0.49	1.52 ± 0.06	2.01 ± 0.72	1.54 ± 0.18
C_{CSF} (nM)	39.1 ± 19.8	116 ± 17**	25.9 ± 12.0	97.1 ± 5.2***	23.1 ± 9.2	43.9 ± 4.1*
C_{brain} (nM)	96.5 ± 27.1	99.9 ± 12.5	85.7 ± 33.8	83.9 ± 10.9	106 ± 30	102 ± 18
$C_{CSF}/C_{p,fu}$ ratio	0.0166 ± 0.005	0.0615 ± 0.0121**	0.0147 ± 0.0046	0.0639 ± 0.0046***	0.0114 ± 0.0027	0.0289 ± 0.0057**

C_p, total plasma concentration; $C_{p,fu}$, unbound plasma concentration; C_{CSF}, CSF concentration; C_{brain}, brain concentration.
* $p < 0.05$, ** $p < 0.01$, and *** $p < 0.001$, significantly different from control rats (unpaired t test).

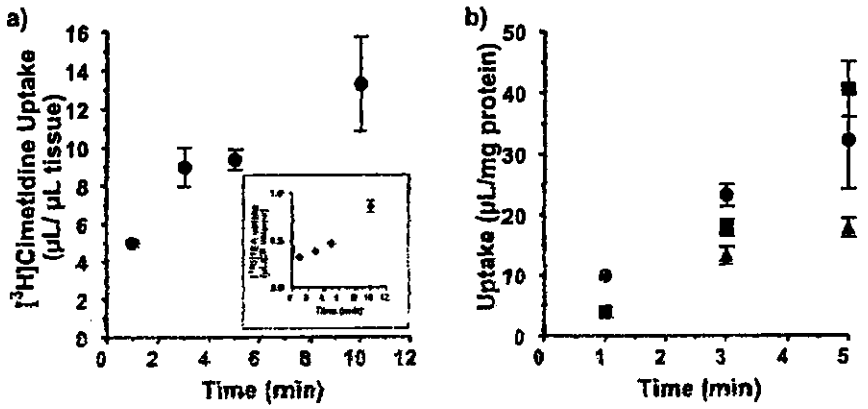

FIG. 5. Uptake of cimetidine, ranitidine, famotidine, and TEA by the isolated rat CP. The rat CP was isolated from the lateral ventricles. a, uptake of [^{3}H]cimetidine (●) and [^{14}C]TEA (◆) by the isolated rat CP was determined by the centrifugal filtration method as described under *Materials and Methods*. The tissue-to-medium concentration ratio of [^{3}H]cimetidine and [^{14}C]TEA was calculated with [^{14}C]urea and [^{3}H]water as cell water space markers, respectively, and corrected for the adherent water space. b, uptake of cimetidine (10 μM; ●), ranitidine (10 μM; ■), and famotidine (10 μM; ▲) by the isolated CP was determined by the rapid filtration method followed by quantification using LC-MS. Each point represents the mean ± S.E. (n = 3).

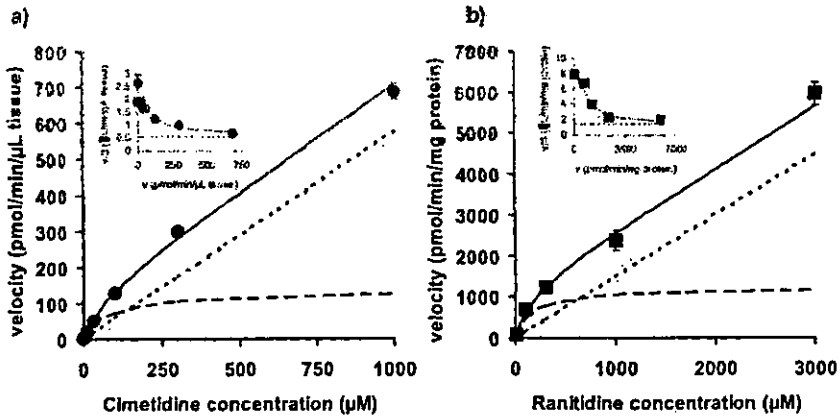

FIG. 6. Concentration dependence of cimetidine and ranitidine accumulation by the isolated rat CP. The accumulation of [^{3}H]cimetidine (a) and ranitidine (b) in the isolated rat CP for 3 and 5 min, respectively, was determined at various substrate concentrations. The concentration dependence for the uptake of [^{3}H]cimetidine and ranitidine is shown as Eadie-Hofstee plots in the inset. Kinetic analyses revealed that the uptake of [^{3}H]cimetidine and ranitidine consists of one saturable and one nonsaturable component and follows the Michaelis-Menten equation. The solid, dotted, and broken lines represent the fitted line, the clearance of the nonsaturable component, and the clearance of the saturable component obtained by nonlinear regression analysis, respectively. Each point represents the mean ± S.E. (n = 3).

its broad substrate specificity for organic anions, from amphipathic to hydrophilic organic anions, and also a weakly basic compound, cimetidine (Kusuhara et al., 1999). In addition to cimetidine, ranitidine was found to be a good substrate of rOat3, whereas famotidine seems to be a poor substrate of rOat3 (Fig. 2). Because it is one of the clues to understanding the interaction of such weak base or cationic compounds with rOat3, the MEP of the H_2-receptor antagonists was calculated (Fig. 1). The H_2-receptor antagonists contain a region of

TABLE 2

Effect of benzylpenicillin and TEA on the uptake of H_2-receptor antagonists by the isolated rat CP

The uptake of cimetidine, ranitidine, and famotidine by isolated rat CP was determined in the presence and absence of benzylpenicillin and TEA at the concentrations indicated. The substrate concentration of cimetidine, ranitidine, and famotidine was 10 μM, and the excess amount of unlabeled substrates represents concentrations of 3, 3, and 1 mM for cimetidine, ranitidine, and famotidine, respectively. Each value represents the mean ± S.E. (n = 3).

	Concentration	Uptake (Percentage of Control)		
		Cimetidine	Ranitidine	Famotidine
	mM			
Control		100 ± 7	100 ± 12	100 ± 22
Excess cold		30.4 ± 1.1	24.8 ± 1.1	50.5 ± 3.6
Benzylpenicillin	0.1	72.5 ± 5.1	76.7 ± 19	83.8 ± 8.3
	1	46.3 ± 1.1	34.9 ± 3.9	78.6 ± 6.6
	3	30.4 ± 1.1	31.8 ± 3.5	51.6 ± 1.9
TEA	0.1	99.5 ± 8.3	94.8 ± 14	120 ± 3
	1	87.5 ± 6.1	97.3 ± 8.6	110 ± 14
	3	93.7 ± 10.5	88.8 ± 13.6	93.4 ± 3.6

negative MEP in their chemical structures (Fig. 1). As Ullrich et al. (1993) suggested, this site might play a key role for the substrate recognition of H_2-receptor antagonists by rOat3. Suzuki et al. (1987) clearly demonstrated a linear correlation between the lipophilicity and reciprocal number of K_i values of β-lactam antibiotics for the uptake of benzylpenicillin by the isolated rat CP. Lipophilicity is likely to be an important factor for recognition by rOat3 in the case of β-lactam antibiotics. In contrast, the kinetic parameters of cimetidine and ranitidine for their uptake by rOat3 were comparable, although they had different cLogD values. Lipophilicity may not be a determinant factor in the case of the H_2-receptor antagonists.

Probenecid has previously been reported to inhibit the apical-to-basal side of azidodeoxythymidine (corresponding to the efflux transport from the CSF side to the blood side under physiological conditions), resulting in an increase in the basal-to-apical transport (Strazielle et al., 2003). Simultaneous administration of probenecid caused a significant increase in the CSF concentration of all the H_2-receptor antagonists examined (Table 1). Since it did not affect the brain and unbound plasma concentrations, it is likely that the effect of probenecid is due to the inhibition of the efflux transport of H_2-receptor antagonists across the CP (Table 1). Strazielle et al. (2003) also found that benzbromarone had an inhibitory effect for the apical-to-basal transport of azidodeoxythymidine. It is possible that benzbromarone treatment also causes an increase in the CSF concentration of H_2-receptor antagonists. Since the brain-to-unbound plasma concentration ratio of the H_2-receptor antagonists was well below unity (Table 1), it is possible that the efflux transport across the brain capillaries limits their brain distribution; however, probenecid had no effect on the brain concentration. Further studies are necessary to investigate whether the H_2-receptor antagonists undergo the efflux across the brain capillaries and whether organic anion transporters, including rOat3, contribute to this efflux.

The uptake, an initial process for elimination from the CSF, was investigated using the isolated rat CP. Time-dependent uptake of the H_2-receptor antagonists was detected in the isolated rat CP (Fig. 5). The saturable component accounts for a large part of the total uptake of cimetidine and ranitidine (Fig. 6). The uptake of cimetidine by the isolated rat CP was markedly inhibited by benzylpenicillin with a K_i value similar to its own K_m value for uptake by the isolated rat CP (Nagata et al., 2002). Conversely, the K_m value of cimetidine for the uptake by the isolated rat CP was similar to its K_i value for the uptake

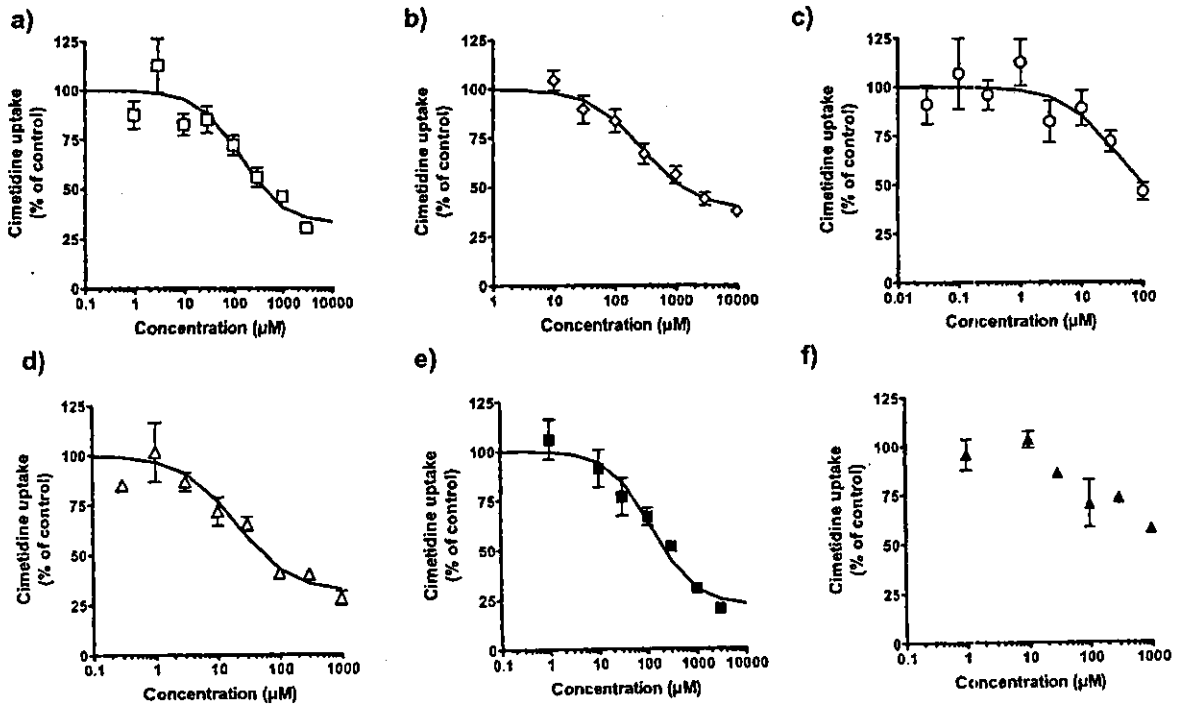

FIG. 7. Inhibitory effect of organic anions and cations on the uptake of cimetidine by the isolated rat CP. The accumulation of [^{3}H]cimetidine (1 μM) by the isolated rat CP for 3 min was determined in the presence and absence of nonradiolabeled compounds at the concentrations indicated. Symbols represent benzylpenicillin (a; □), PAH (b; ◇), estradiol-17β-glucuronide (c; ○), estrone sulfate (d; △), ranitidine (e; ■), and famotidine (f; ▲). The solid lines represent the fitted line obtained by nonlinear regression analysis. The details of the fitting are described under *Materials and Methods*. Each point represents the mean ± S.E. (n = 3).

TABLE 3

K_i and K_m values for the uptake of cimetidine, ranitidine, and benzylpenicillin by the isolated rat CP

The effect of estrone sulfate, cimetidine, estradiol-17β-glucuronide ($E_2$17βG), PAH, benzylpenicillin, and ranitidine was examined with regard to uptake by the rat isolated CP. The K_i and K_m values were determined by nonlinear regression analysis as described under *Materials and Methods*. Data are taken from Fig. 7. Each value represents the mean ± S.E. (n = 3–6).

	K_i and K_m values (μM)		
	Benzylpenicillin[a]	Cimetidine	Ranitidine
Estrone sulfate	22.3	19.5 ± 8.8	
Cimetidine	44.4	92.7 ± 46.1[b]	
$E_2$17βG	33.0	36.3 ± 15.7	
PAH	406	281 ± 74	
Benzylpenicillin	111[b]	140 ± 97	
Ranitidine		49.6 ± 15.1	171 ± 57[b]

[a] Parameters cited from Nagata et al. (2002).
[b] K_m value.

of benzylpenicillin by the isolated CP (Table 3; Nagata et al., 2002). Furthermore, the inhibition constants of the compounds listed in Table 3, which are substrates of rOat3, are similar for the uptake of cimetidine and benzylpenicillin by the isolated rat CP (Table 3). These results suggest that the same organic anion transporter, namely, rOat3, is responsible for the uptake of cimetidine by the isolated rat CP. Since the K_i value of ranitidine for the uptake of cimetidine was close to its K_m value (Table 3) and benzylpenicillin showed similar inhibition potency (Table 2), rOat3 is presumably also involved in the uptake of ranitidine. Since the uptake of famotidine was saturable and inhibited by benzylpenicillin (Table 2), the involvement of a transporter was suggested, although the fraction of the saturable component could not be precisely estimated due to its limited solubility. This is consistent with the in vivo result. Since famotidine is a poor substrate of rOat3, the benzylpenicillin-sensitive fraction of famotidine uptake may at least partly be accounted for by rOat3; however, it is possible that other transporters distinct from rOat3 and organic cation transporter may play a major role in the uptake of famotidine by the isolated rat CP. Villalobos et al. (1997) demonstrated the presence of a membrane potential-sensitive uptake mechanism for hydrophilic organic cations at the primary cultured CP epithelial cells. Reverse transcription-polymerase chain reaction analyses detected mRNA expression of Oct2 and Oct3 in the CP, and this may account for the uptake of hydrophilic organic cations in the CP (Sweet et al., 2001). The expression level of rOct2 in the CP was considerably lower than that in the kidney, whereas that of rOct3 was the same for all the tissues examined, although the absolute value was low (Choudhuri et al., 2003). The low expression of Oct mRNA may account for the lower uptake of TEA by the isolated rat CP compared with that of the H_2-receptor antagonists (Fig. 5). Although cimetidine is a substrate of rOct2 (Grundemann et al., 1999), the effect of TEA on the uptake of the H_2-receptor antagonists by the isolated rat CP was minimal, even at a concentration sufficient to saturate TEA uptake by primary cultured choroid epithelial cells (Table 2) (Villalobos et al., 1997). Therefore, the contribution of rOcts to the total uptake of H_2-receptor antagonists by the isolated rat CP is minimal, although they are involved.

rOat3 has been shown to be expressed on the basolateral membrane of the proximal tubules and involved in the uptake of organic anions (Hasegawa et al., 2002, 2003). However, probenecid treatment did not affect the steady-state plasma concentration of H_2-receptor antagonists, although the unbound plasma concentration was sufficient to inhibit rOat3-mediated uptake (Table 1). This result is in a good agreement with the previous report by Boom and Russel (1993). They examined the uptake of cimetidine by freshly isolated rat proximal tubular cells and demonstrated that the major fraction of cimetidine uptake (approximately 50%) was inhibited by TEA (Boom and Russel, 1993). Probenecid was only a weak inhibitor, with an IC_{50} value (700 μM) greater than the unbound plasma concentration employed in this study. Organic cation transporter(s) will play a major role in the renal uptake of cimetidine, whereas the uptake by the isolated rat CP is totally accounted for by the organic anion transporter. This unique phenomenon is entirely due to the unique nature of the bisubstrate, which is a substrate of both organic anion and cation transporters.

The results of the present study suggest the possibility of drug-drug interactions between the H_2-receptor antagonists and organic anions that cause an increase in the CSF concentration of H_2-receptor antagonists without affecting their plasma concentration profiles, as in the case of probenecid. The risk of mental confusion with cimetidine in patients with renal or hepatic dysfunction is higher than that in normal patients (Schentag et al., 1981). Furthermore, Schentag et al. (1979) reported that the concentration of cimetidine in the CSF is related to the mental status. The $C_{CSF}/C_{p,fu}$ ratio in patients with hepatic dysfunction was 2-fold greater than normal patients, whereas the plasma clearance by both types of patients was not significantly different (Schentag et al., 1979, 1981). These phenomena might be attributed to the inhibition of the efflux transport across the CP by endogenous compounds accumulated in the body due to hepatic dysfunction. Indeed, some organic anions (e.g., quinolinic acid) are known to be elevated in the CSF of patients with hepatic dysfunction (Moroni et al., 1986).

In conclusion, cimetidine and ranitidine are good substrates for rOat3, whereas famotidine is a poor substrate for this transporter. The efflux transport across the CP plays an important role in regulating the CSF concentration of H_2-receptor antagonists. rOat3 is the most likely candidate transporter for the uptake of H_2-receptor antagonists by the isolated rat CP.

References

Boom SP and Russel FG (1993) Cimetidine uptake and interactions with cationic drugs in freshly isolated proximal tubular cells of the rat. *J Pharmacol Exp Ther* 267:1039–1044.

Burckhardt BC and Burckhardt G (2003) Transport of organic anions across the basolateral membrane of proximal tubule cells. *Rev Physiol Biochem Pharmacol* 146:95–158.

Choudhuri S, Cherrington NJ, Li N, and Klaassen CD (2003) Constitutive expression of various xenobiotic and endobiotic transporter mRNAs in the choroid plexus of rats. *Drug Metab Dispos* 31:1337–1345.

Dantzler WH and Wright SH (2003) The molecular and cellular physiology of basolateral organic anion transport in mammalian renal tubules. *Biochim Biophys Acta* 1618:185–193.

Ghersi-Egea JF and Strazielle N (2001) Brain drug delivery, drug metabolism and multidrug resistance at the choroid plexus. *Microsc Res Tech* 52:83–88.

Grimson T (1977) Reactions to cimetidine. *Lancet* 1:858.

Grundemann D, Liebich G, Kiefer N, Koster S, and Schomig E (1999) Selective substrates for non-neuronal monoamine transporters. *Mol Pharmacol* 56:1–10.

Hasegawa M, Kusuhara H, Endou H, and Sugiyama Y (2003) Contribution of organic anion transporters to the renal uptake of anionic compounds and nucleoside derivatives in rat. *J Pharmacol Exp Ther* 305:1087–1097.

Hasegawa M, Kusuhara H, Sugiyama D, Ito K, Ueda S, Endou H, and Sugiyama Y (2002) Functional involvement of rat organic anion transporter 3 (rOat3; Slc22a8) in the renal uptake of organic anions. *J Pharmacol Exp Ther* 300:746–753.

Haselbach M, Wegener J, Decker S, Engelbertz C, and Galla HJ (2001) Porcine choroid plexus epithelial cells in culture: regulation of barrier properties and transport processes. *Microsc Res Tech* 52:137–152.

Kusuhara H, Sekine T, Utsunomiya-Tate N, Tsuda M, Kojima R, Cha SH, Sugiyama Y, Kanai Y, and Endou H (1999) Molecular cloning and characterization of a new multispecific organic anion transporter from rat brain. *J Biol Chem* 274:13675–13680.

Kusuhara H and Sugiyama Y (2001) Efflux transport systems for drugs at the blood-brain barrier and blood-cerebrospinal fluid barrier (Part 1). *Drug Discov Today* 6:150–156.

McGuigan J (1981) A consideration of the adverse effects of cimetidine. *Gastroenterology* 80:181–192.

Moroni F, Lombardi G, Carla V, Lal S, Etienne P, and Nair N (1986) Increase in the content of quinolinic acid in cerebrospinal fluid and frontal cortex of patients with hepatic failure. *J Neurochem* 47:1667–1671.

Nagata Y, Kusuhara H, Endou H, and Sugiyama Y (2002) Expression and functional characterization of rat organic anion transporter 3 (rOat3) in the choroid plexus. *Mol Pharmacol* 61:982–988.

Schentag JJ, Cerra FB, Calleri G, DeGlopper E, Rose JQ, and Bernhard H (1979) Pharmacokinetic and clinical studies in patients with cimetidine-associated mental confusion. *Lancet* 1:177–181.

Schentag JJ, Cerra FB, Calleri GM, Leising ME, French MA, and Bernhard H (1981) Age,

disease and cimetidine disposition in healthy subjects and chronically ill patients. *Clin Pharmacol Ther* 29:737–743.
Segal MB (2000) The choroid plexuses and the barriers between the blood and the cerebrospinal fluid. *Cell Mol Neurobiol* 20:183–196.
Strazielle N, Belin MF, and Ghersi-Egea JF (2003) Choroid plexus controls brain availability of anti-HIV nucleoside analogs via pharmacologically inhibitable organic anion transporters. *AIDS* 17:1473–1485.
Sugiyama D, Kusuhara H, Shitara Y, Abe T, Meier PJ, Sekine T, Endou H, Suzuki H, and Sugiyama Y (2001) Characterization of the efflux transport of 17beta-estradiol-D-17beta-glucuronide from the brain across the blood-brain barrier. *J Pharmacol Exp Ther* 298:316–322.
Suzuki H, Sawada Y, Sugiyama Y, Iga T, and Hanano M (1985) Saturable transport of cimetidine from cerebrospinal fluid to blood in rats. *J Pharmacobio-Dyn* 8:73–76.
Suzuki H, Sawada Y, Sugiyama Y, Iga T, and Hanano M (1986) Transport of cimetidine by the rat choroid plexus in vitro. *J Pharmacol Exp Ther* 239:927–935.
Suzuki H, Sawada Y, Sugiyama Y, Iga T, and Hanano M (1987) Transport of benzylpenicillin by the rat choroid plexus in vitro. *J Pharmacol Exp Ther* 242:660–665.
Suzuki H, Sawada Y, Sugiyama Y, Iga T, and Hanano M (1988) Efflux of cimetidine from the rat cerebrospinal fluid. *Drug Metab Dispos* 16:328–330.
Suzuki H, Terasaki T, and Sugiyama Y (1997) Role of efflux transport across the blood-brain barrier and blood cerebrospinal fluid barrier on the disposition of xenobiotics in the central nervous system. *Adv Drug Delivery Rev* 25:257–285.
Sweet DH, Miller DS, and Pritchard JB (2001) Ventricular choline transport: a role for organic cation transporter 2 expressed in choroid plexus. *J Biol Chem* 276:41611–41619.
Sweet DH, Miller DS, Pritchard JB, Fujiwara Y, Beier DR, and Nigam SK (2002) Impaired organic anion transport in kidney and choroid plexus of organic anion transporter 3 (Oat3 (Slc22a8)) knockout mice. *J Biol Chem* 277:26934–26943.
Ullrich KJ, Rumrich G, David C, and Fritzsch G (1993) Bisubstrates: substances that interact with renal contraluminal organic anion and organic cation transport systems. I. Amines, piperidines, piperazines, azepines, pyridines, quinolines, imidazoles, thiazoles, guanidines and hydrazines. *Pflugers Arch* 425:280–299.
Villalobos AR, Parmelee JT, and Pritchard JB (1997) Functional characterization of choroid plexus epithelial cells in primary culture. *J Pharmacol Exp Ther* 282:1109–1116.
Yamaoka K, Tanigawara Y, Nakagawa T, and Uno T (1981) A pharmacokinetic analysis program (multi) for microcomputer. *J Pharmacobio-Dyn* 4:879–885.

Address correspondence to: Dr. Yuichi Sugiyama, Graduate School of Pharmaceutical Sciences, the University of Tokyo, 7-3-1, Hongo, Bunkyo-ku, Tokyo 113-0033, Japan. E-mail: sugiyama@mol.f.u-tokyo.ac.jp

0022-3565/04/3093-1282–1290$20.00
THE JOURNAL OF PHARMACOLOGY AND EXPERIMENTAL THERAPEUTICS

JPET 309:1282–1290, 2004

Vol. 309, No. 3
61671/1152644
Printed in U.S.A.

Isolation and Characterization of a New Major Intestinal CYP3A Form, CYP3A62, in the Rat

T. Matsubara, H. J. Kim, M. Miyata, M. Shimada, K. Nagata, and Y. Yamazoe

Division of Drug Metabolism and Molecular Toxicology, Graduate School of Pharmaceutical Sciences, Tohoku University, Sendai, Japan

Received October 19, 2003; accepted March 4, 2004

ABSTRACT

Based on information of the nucleotide sequence obtained from rat genome clones, a new CYP3A (CYP3A62) cDNA was isolated from the cDNA library of a rat liver. The CYP3A62 cDNA was 1746 base pairs (bp) in length, which included 1491 bp of an open reading frame and 93 bp and 209 bp of the respective 5′- and 3′-noncoding regions. Amino acid sequence deduced from CYP3A62 cDNA shared the highest similarity with rat CYP3A9 (79.9%) among human and rat CYP3A forms previously reported. CYP3A62 mRNA and protein were consistently detected in small intestines as well as livers. CYP3A62 was a major form in small intestines of both sexes but was a female-predominant form in livers of adult rats. CYP3A62 in both tissues of male and female rats were clearly enhanced by the treatment with dexamethasone. These expression profiles resembled those of CYP3A9. Despite clear detection of CYP3A62, no detectable levels of CYP3A1 and CYP3A2 proteins, as well as those of mRNAs, were found in the intestinal tract. Therefore, CYP3A62 may play major roles together with CYP3A9 and CYP3A18 in endogenous or exogenous detoxification at the absorption site.

The CYP3A subfamily consists of several forms that display considerable extents of similarity with one another in their molecular weights, immunochemical properties, and substrate specificities (Gonzalez, 1988; Nelson et al., 1996). Human CYP3A forms metabolize more than about half of therapeutic drugs (Cholerton et al., 1992; Li et al., 1995) and are also involved in the metabolism of endogenous chemicals such as bile acids (Araya and Wikvall, 1999), steroid hormones (Waxman et al., 1988), and retinoic acid (Marill et al., 2000). CYP3A forms are expressed predominantly in the liver but are also found in other organs such as the gut (Kolars et al., 1994), white blood cells (Janardan et al., 1996; Sempoux et al., 1999), and brain (Wang et al., 1996). The level of CYP3A4 in the intestine is reported to share more than 50% of the total cytochrome P450 (P450) content (Zhang et al., 1999).

In rats, CYP3A1 (Gonzalez et al., 1985), CYP3A2 (Gonzalez et al., 1986), CYP3A9 (Wang et al., 1996), CYP3A18 (Strotkamp et al., 1995; Nagata et al., 1996), and CYP3A23 (Kirita and Matsubara, 1993; Komori and Oda, 1994) have been reported as rat CYP3A forms. CYP3A23 was, however, identified to be the same form as CYP3A1 by analysis of the *CYP3A1* gene (Nagata et al., 1999). These CYP3A forms appear in a sex-dependent manner in rats. For example, CYP3A2 (Yamazoe et al., 1988; Cooper et al., 1993) and CYP3A18 (Nagata et al., 1996; Robertson et al., 1998) are male-specific forms, whereas CYP3A9 is a female-dominant form (Wang and Strobel, 1997; Robertson et al., 1998). The expression profiles in the intestinal tract, however, are obscure with all of the forms.

Levels of CYP3A forms are enhanced after treatment with structurally diverse compounds such as dexamethasone, clotrimazole, and rifampicin (Hostetler et al., 1989; Daujat et al., 1991; Burger et al., 1992; Kocarek et al., 1995). Intestinal CYP3A forms play important roles on the first-pass effect of drugs. In humans, however, rather distinct controls of hepatic and small intestinal CYP3A4s were suggested from experiments using CYP3A4 probe drugs and also from the protein levels. Thus, an understanding of their enzymatic and molecular biological properties is necessary before predicting drug-drug interaction.

As the results of the genome sequencing in various experimental animal species, a number of unidentified genes have been found to provide the information of a novel protein. We have previously isolated six different *CYP3A*-related DNA clones from a rat genomic library (K. Nagata, T. Matsubara, and Y. Yamazoe, unpublished data). The four DNA clones contained information on a part of the first exon boundary of

Article, publication date, and citation information can be found at http://jpet.aspetjournals.org.
DOI: 10.1124/jpet.103.061671.

ABBREVIATIONS: P450, cytochrome P450; PCR, polymerase chain reaction; PAGE, polyacrylamide gel electrophoresis; G6PDH, glucose-6-phosphate dehydrogenase; RT-PCR, reverse transcription-polymerase chain reaction; bp, base pair; HNF-4α, hepatocyte nuclear factor-4α.

CYP3A1, *CYP3A2*, *CYP3A9*, and *CYP3A18* genes, whereas the other two remained unidentified.

In the present study, we have isolated a novel CYP3A cDNA encoding CYP3A62 from rat liver cDNAs. We have also characterized enzymatic and molecular biological properties of this new form in comparison with the other four rat CYP3A forms.

Materials and Methods

Materials. Restriction endonucleases and enzymes were purchased from Takara (Kyoto, Japan). Alkaline phosphatase-conjugated goat anti-rabbit IgG was purchased from Sigma-Aldrich (St. Louis, MO). A mammalian expression vector, pCMV4, was provided by Dr. David W. Russell (University of Texas Southwestern Medical Center, Dallas, TX). Dulbecco's modified Eagle's medium and fetal calf serum were obtained from Invitrogen (Carlsbad, CA), and other chemicals were obtained from Sigma-Aldrich and Wako Pure Chemicals (Osaka, Japan).

Isolation and Sequencing of CYP3A62 cDNA. Oligonucleotide primers used for isolation of CYP3A62 cDNA were 5′-GCAGCACACACAAGCTAAGAA-3′ (fragment 1), 5′-CTGTGACCTATGATGTCCTG-3′ (fragment 2), and 5′-AGCAGCAATGGACCTGATCC-3′ (fragment 3) for the forward primers, and 5′-GAGAGCAAACCTCATGCC-3′ (fragment 1), 5′-TTTTTTTTTTTTTTTTT-3′ (fragment 2), and 5′-CCACTCATGGTTCAATC-3′ (fragment 3) for the reverse primers, respectively. DNA fragments from the liver cDNAs of a male adult rat were amplified by the use of Takara *Taq* (Takara, Kyoto, Japan). The reaction mixture (30 μl) contained 1 μl of the template DNA solution, 20 pmol of each of the forward and reverse primers, 250 μM dATP, dCTP, dTTP, and dGTP each, and 1 unit of *Taq* polymerase. After initial denaturation at 94°C for 5 min, the amplification was carried out for 30 cycles with 0.5 min at 94°C for denaturation, 1 min at 55°C for annealing, 1.5 min at 72°C for extension, and a final extension period of 7 min at 72°C.

Transfection of CYP3As into COS-1 Cells and Expression of CYP3A Forms. Constructions of plasmids for CYP3A62, CYP3A9, and CYP3A18 cDNAs were carried out by insertion between the *Mlu*I and *Bgl*II sites of pCMV4; constructions of plasmids for CYP3A1 and CYP3A2 cDNAs were carried out by insertion into the *Eco*RI sites of p91023(B) as reported previously under *Methods* (Miyata et al., 1994; Nagata et al., 1999). These cDNAs were isolated from rat male DNA libraries using a PCR method. These plasmid constructs (50 μg) were transfected into COS-1 cells (2.0×10^6 cells) using an electroporation method. The COS-1 cells cultured at 37°C for 72 h were collected in 2 ml of phosphate-buffered saline. The precipitated cells were resuspended in 100 μl of 75 mM potassium phosphate buffer (pH 7.4) after centrifugation at 2000*g* for 5 min and then homogenized. The homogenate was centrifuged at 9000*g* for 20 min. The supernatant was further centrifuged at 105,000*g* for 60 min, and the microsomal pellet was resuspended in 50 μl of buffer (20% glycerol in 0.1 M potassium phosphate buffer; pH 7.4). Cytochrome P450 content was estimated by the method of Omura and Sato (1964).

Treatment of Animals and Preparation of Microsomes. Male and female Sprague-Dawley rats (10 weeks old) purchased from Japan SLC (Shizuoka, Japan) were acclimated for 3 days. They were divided into three groups (control, dexamethasone-treated, and lithocholic acid-treated). Dexamethasone suspended in corn oil was given intraperitoneally to rats at a dose of 100 mg/kg/day for 3 consecutive days. Lithocholic acid was given orally at a dose of 100 mg/kg/day for 3 consecutive days. Corn oil (1 ml/head) was given to the controls. Microsomes and total RNAs were prepared 20 h after the last dose. Microsomes were prepared as previously described (Yamazoe et al., 1986). Intestinal mucosa microsomes were prepared as follows. The small intestine removed was immediately placed in liquid nitrogen. The tissue cut into small pieces was added to ice-cold buffer (75 mM potassium phosphate buffer, pH 7.4, containing 1 mM EDTA, 1 mM phenylmethylsulfonyl fluoride, 100 μg/ml trypsin inhibitor, and 19 μg/ml aprotinin). The microsomal fraction was isolated using the procedure described for liver microsomes. Microsomal protein was determined by the method of Lowry et al. (1951).

Immunoblot Analysis. Microsomal proteins were electrophoresed in 16 cm of a 7.5% SDS-PAGE for separation and 1 cm of a 2.0% SDS-PAGE for stacking and transferred to a nitrocellulose membrane. The sheet was immunostained with human anti-CYP3A antibody prepared as described previously (Kawano et al., 1987), alkaline phosphatase-conjugated goat anti-rabbit IgG, 5-bromo-4-chloro-3-indolylphosphate, and nitro blue tetrazonium as described previously (Blake et al., 1984).

Testosterone Hydroxylation. The reaction mixture for measurement of testosterone 6β-hydroxylase activities consists of 50 μg of protein of COS-1 microsomes expressing a CYP3A form, 100 mM potassium phosphate buffer (pH 7.4), 5 pmol of cytochrome b_5, 0.1 unit (0.1 nmol of cytochrome *c* per minute) of NADPH-P450 reductase, and 5 μg of sodium cholate in a final volume of 100 μl. The reaction was started by the addition of NADPH (final concentration, 0.5 mM) and terminated by adding ethyl acetate after 40 min of incubation at 37°C. Testosterone hydroxylation was quantified by the method described previously (Yamazoe et al., 1988; Guo et al., 2000).

Amiodarone and Lidocaine De-ethylations. The reaction mixtures for amiodarone and lidocaine *N*-de-ethylase activities consisted of 50 μg of protein of COS-1 microsomes expressing a CYP3A form, 100 mM potassium phosphate buffer (pH 7.4), 5 pmol of cytochrome b_5, 0.1 unit of NADPH-P450 reductase, 5 μg of sodium cholate, and 200 nmol of amiodarone or lidocaine in a final volume of 100 μl. The reaction was started by the addition of NADPH (final concentration, 0.5 mM) and then terminated by the addition of zinc sulfate and barium hydroxide after 40 min of incubation at 37°C. The acetaldehyde thus formed was converted to a decahydroacridine derivative using the reaction with 4 μg of 1,3-cyclohexandione, 4 mg of ammonium acetate, and 2 mg of acetic acid at 80°C for 30 min in a final volume of 300 μl. The derived product was quantified using a high-performance liquid chromatography system equipped with a C_{18} reversed-phase analytical column (particle size, 7 μm, 4.6 × 150 mm). The metabolites were detected with the fluorescence at excitation and fluorescence wavelengths of 390 and 457 nm, respectively. The sample was eluted using acetonitrile/0.5% acetic acid in distilled water (1:4) at a flow rate of 1 ml/min.

Analysis of Rat CYP3A mRNAs. Total RNA was extracted from the following tissues: liver, kidney, spleen, lung, heart, adrenal, brain, stomach, duodenum, jejunum, ileum, colon, testis, prostate, ovary, and uterus of male and female rats using an acid guanidinium

TABLE 1
Primer used in PCR reaction for mRNA detection and quantification

Messenger	Forward Primer	Reverse Primer	Fragment Size
CYP3A62	5′-GGAGATAAAGAGTCTCACC-3′	5′-AGTTCTGCAGGACTCAGAC-3′	544
CYP3A1	5′-GCAGATCACAGCCCAGTCAATC-3′	5′-TGGCCAGTGCTGTGGATCAC-3′	349
CYP3A2	5′-CAAGGGAGATGTTCCCCATCATTG-3′	5′-GCTATGATTTCAACATCAGAC-3′	469
CYP3A9	5′-CCATAACATCAATCCTTATATG-3′	5′-GCACGCGTGATACAACACCACTATAGGC-3′	276
CYP3A18	5′-CCAATCTATCCTCTTCATCGGA-3′	5′-CCCCGGGAAATTCACTGTCC-3′	326
G6PDH	5′-GAAGCAGTCACCAAGAAC-3′	5′-CTGCATGACATCCCTGATGATC-3′	332

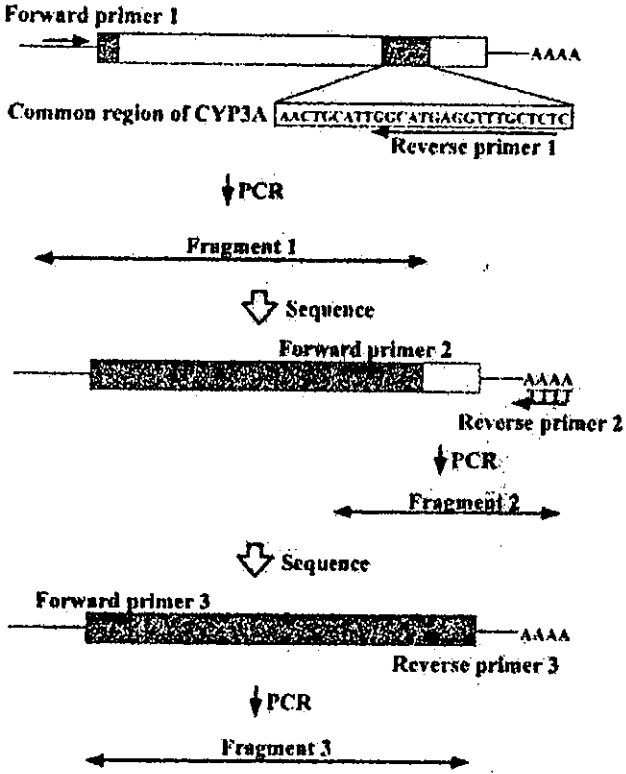

Fig. 1. The strategy for isolation of CYP3A62 cDNA. Boxes represent the cording region. Identified or predicted regions are shown as hatched.

thiocyanate-phenol-chloroform method. Total RNAs of each tissue were combined for a pool of four individuals. The cDNA was reverse-transcripted from those total RNAs with Ready-To-Go (Amersham Biosciences Inc., Piscataway, NJ). The nucleotide sequences of CYP3A62-, CYP3A1-, CYP3A2-, CYP3A9-, CYP3A18-, and G6PDH-selective oligonucleotide primers are shown in Table 1. cDNA fragments for CYP3A62, CYP3A1, CYP3A2, CYP3A9, CYP3A18, and G6PDH were amplified by use of Takara *Taq*. The reaction mixture (30 μl) contained 1 μl of the cDNA solution as a template DNA, 20 pmol of each forward and reverse primer as described above, 250 μM dATP, dCTP, dTTP, and dGTP each, 1 unit each of the enzyme and the buffer. After initial denaturation at 94°C for 5 min, the targeted nucleotides were amplified for 35 cycles (RT-PCR) or 40 cycles (real-time PCR), with 30 s at 94°C for denaturation, 15 s at 55°C (CYP3A9 and G6PDH), 60°C (CYP3A62 and CYP3A2), or 63°C (CYP3A1 and CYP3A18) for annealing, 30 s at 72°C for extension, and a final extension period of 7 min at 72°C. The quantification of mRNAs was carried out with SYBR Green by using ABI PRISM 7000 (Applied Biosystems, Foster City, CA). A real-time PCR method was used to determine the expression amounts of CYP3A mRNAs in various rat tissues. In these experiments, levels of CYP3A mRNAs were normalized from the amount of total RNA.

Results

Isolation and Analysis of CYP3A62 cDNA. In previous experiments, we have identified six different promoter regions of CYP3A genes from rats. Four of them were matched to genes encoding the first exon regions of CYP3A forms [(*CYP3A1* (Gonzalez et al., 1985), *CYP3A2* (Gonzalez et al., 1986), *CYP3A9* (Wang et al., 1996), and *CYP3A18* (Nagata et al., 1996), respectively] that were identified previously. The other two clones seemed to encode unknown CYP3A genes. Based on this information, a novel CYP3A form (CYP3A62) cDNA has been isolated using RT-PCR. A fragment 1 of CYP3A62 cDNA was at first amplified from the liver cDNA of a male adult rat with the forward primer 1 and reverse primer 1 (Fig. 1), and the nucleotide sequence was deter-

TABLE 2

Homology of amino acid sequence among CYP3A forms. CYP3A1, K. Nagata (L24207); CYP3A2, M. Miyata (NM_153312); CYP3A9, P. Nef (NM_147206); CYP3A18, K. Nagata (NM_145782); CYP3A4, T. Molowa (NM_017460); CYP3A5, T. Aoyama (NM_000777); CYP3A7, M. Komori (NM_000765); CYP3A43, T. L. Domonski (AF319634).

	CYP3A1	CYP3A2	CYP3A9	CYP3A18	CYP3A4	CYP3A5	CYP3A7	CYP3A43
CYP3A62	69.3	67.7	79.9	67.2	71.6	73.4	69.8	67.0
CYP3A1		86.3	72.6	69.7	71.8	71.6	68.8	63.1
CYP3A2			72.2	67.1	72.0	70.8	69.2	63.5
CYP3A9				68.4	76.5	75.1	72.8	68.0
CYP3A18					68.4	68.6	65.2	64.4
CYP3A4						84.3	88.3	75.7
CYP3A5							81.9	75.7
CYP3A7								71.4

TABLE 3

The quantification of male and female rat CYP3A mRNAs by real-time PCR in liver and intestinal tract. Real-time PCR was carried out as described under *Materials and Methods*. The numbers represent the molecular number of CYP3A mRNA to total RNA amount (attomole of CYP3A mRNA/μg total RNA). The limit of detectable CYP3A mRNAs was less than 0.01 attomoles of CYP3A mRNA/μg of total RNA.

Sex	Tissue	Cytochrome P450				
		CYP3A62	CYP3A1	CYP3A2	CYP3A9	CYP3A18
Male	Liver	1.05	52.48	382.69	3.97	6.29
	Duodenum	9.61	N.D.	N.D.	12.42	0.39
	Jejunum	7.88	N.D.	N.D.	8.49	0.55
	Ileum	5.50	N.D.	N.D.	1.11	0.25
	Colon	3.01	N.D.	N.D.	0.89	0.04
Female	Liver	5.73	39.09	N.D.	12.94	0.97
	Duodenum	7.27	N.D.	N.D.	0.61	0.10
	Jejunum	2.54	N.D.	N.D.	0.11	0.10
	Ileum	1.09	N.D.	N.D.	0.04	0.07
	Colon	0.24	N.D.	N.D.	0.14	N.D.

N.D., not detectable.

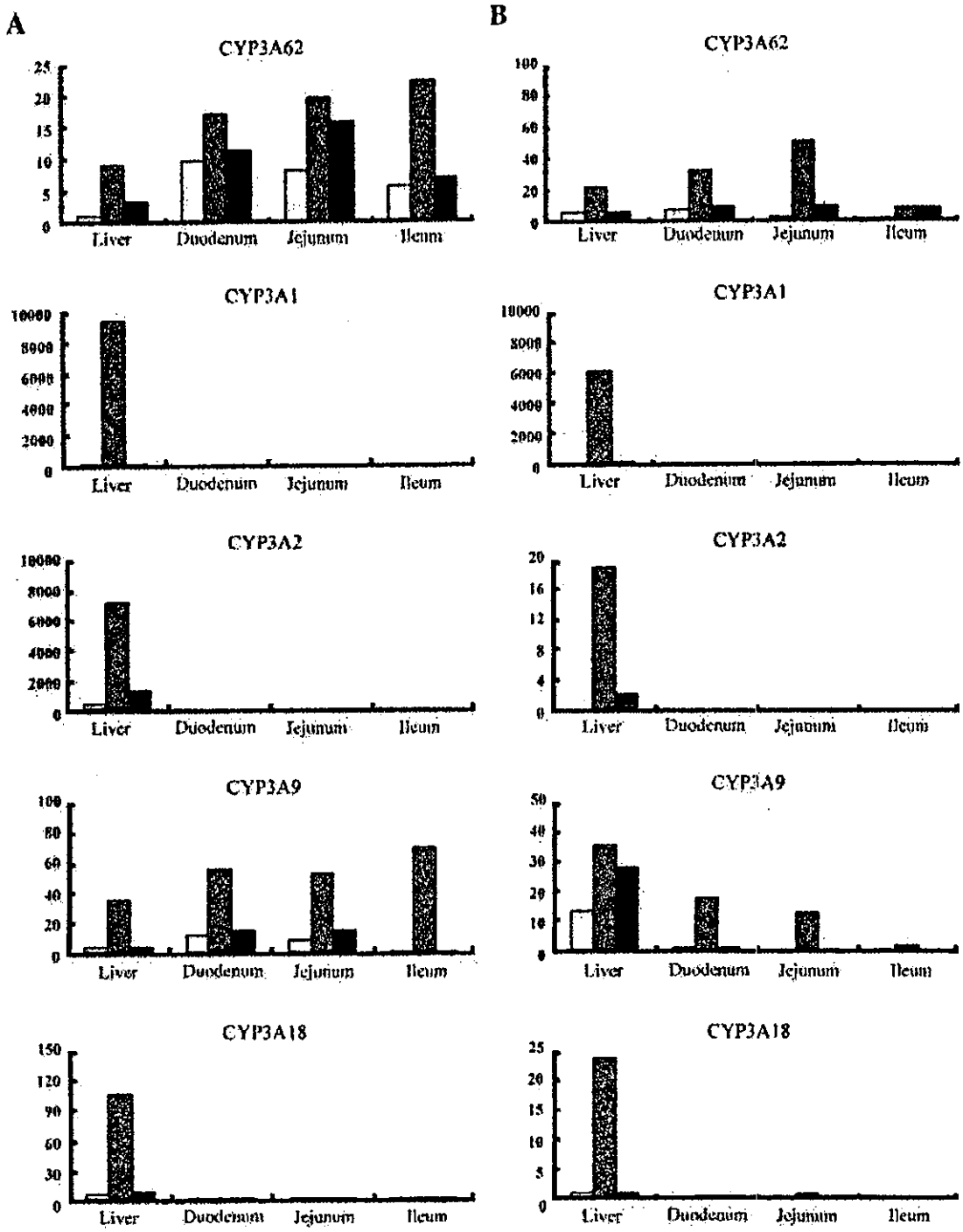

Fig. 2. Changes in the profile of rat CYP3A mRNAs after treatment with dexamethasone or lithocholic acid in liver and intestinal tract. Real-time PCR and drug treatment were carried out as described under *Materials and Methods*. A, male rat; B, female rat. Semiclosed column, closed column, and open column represent the rat group treated with dexamethasone, treated with lithocholic acid, and the control group, respectively. The numbers in this figure represent the molecular number of CYP3A mRNA to total RNA amount (attomole per microgram). The limit of detectable CYP3A mRNAs was less than 0.01 attomoles of CYP3A mRNA/μg total RNA.

mined. The reverse primer 1 was constructed from a region of highly conserved nucleotide sequences among CYP3A cDNAs. Second, a fragment 2 was amplified with the forward primer 2 and reverse primer 2 to determine the nucleotide sequence. Finally, fragment 3 of the CYP3A62 cDNA, including an entire open reading frame, was amplified from the rat liver cDNAs with the forward primer 3 and reverse primer 3. The nucleotide sequence of fragment 3 was completely identical with those of fragments 1 and 2 (Fig. 1). In this strategy, the identified cDNA was 1746 bp in length, which had an open reading frame of 1491 bp (corresponding to 497 amino acids), 93 bp and 209 bp of the 5′- and 3′-noncoding regions,

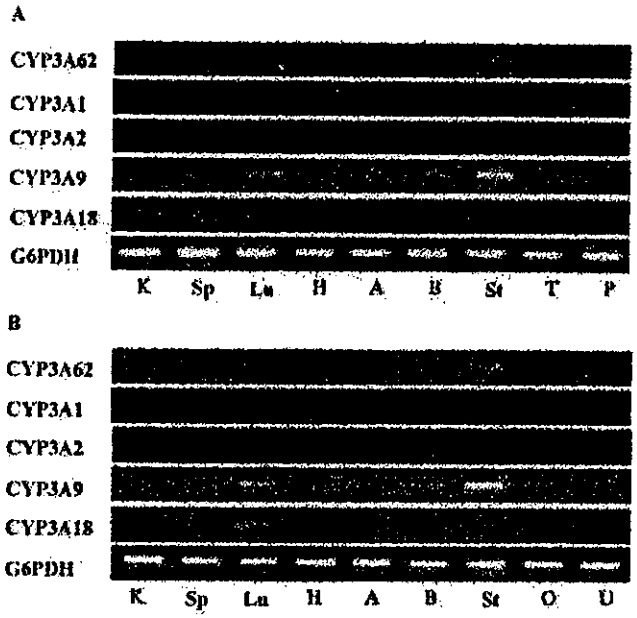

Fig. 3. Detection of rat CYP3A mRNAs in tissues other than liver and intestine. RT-PCR was carried out as described under *Materials and Methods*. Electrophoresis was performed in a 1% agarose gel. A, male rat tissues; B, female rat tissues. Lanes: K, kidney; Sp, spleen; Lu, lung; H, heart; A, adrenal; B, brain; St, stomach; Te, testis; P, prostate; O, ovary; U, uterus.

respectively. This nucleotide sequence was deposited with the DDBJ nucleotide sequence database (Accession no. AB084894). CYP3A62 cDNA showed the highest similarity in the nucleotide sequence with rat CYP3A9 and mouse Cyp3a13 cDNAs (both 84.4%). CYP3A62 showed the highest similarity with CYP3A9 (79.9%) and also showed 67.0 to 73.4% similarity in amino acid sequence with other rat and human CYP3A forms (Table 2). A unique property of this new form is in the number of cording residues. A nucleotide change (change A to T) at 1584 bp of CYP3A62 cDNA to form a termination codon resulted in 3- or 6-amino acid shorter sequences as compared with those of other CYP3A forms except for CYP3A18.

Quantification of CYP3A mRNAs in Liver and Intestinal Tract. The quantification of individual CYP3A mRNAs was carried out by the use of a real-time PCR method. As shown in Table 3, predominant expression of CYP3A62 mRNA and CYP3A9 mRNA in the female over the male was observed in the liver. The level of CYP3A62 mRNA was about 5 times higher in the female than in the male in liver (5.73 and 1.05 attomole/μg total RNA, respectively). CYP3A62 mRNA was also detected in the intestinal tract of both sexes. The level was rather higher in the male intestinal tract than in the liver (duodenum, jejunum, ileum, and colon were 9.61, 7.88, 5.50, and 3.01 attomole/μg total RNA, respectively). In female rats, the level was roughly equivalent between the liver and duodenum (5.73 and 7.27 attomole/μg total RNA, respectively), and lower in the jejunum, ileum, and colon than in the duodenum (jejunum, ileum, and colon were 2.54, 1.09, and 0.24 attomole/μg total RNA, respectively). Their tissue distribution profiles were similar to those of CYP3A9 mRNA. CYP3A2 and CYP3A18 mRNAs were predominantly expressed in male rat livers as previously reported (Cooper et al., 1993; Robertson et al., 1998). The amount of CYP3A2 mRNA was highest among rat CYP3A forms (382.69 attomole/μg total RNA). CYP3A1 mRNA was also observed in livers of both sexes (male and female were 52.48 and 39.09 attomole/μg total RNA, respectively), although the levels were lower than that of CYP3A2 mRNA in male rats. An interesting thing is that CYP3A1 and CYP3A2 mRNAs were

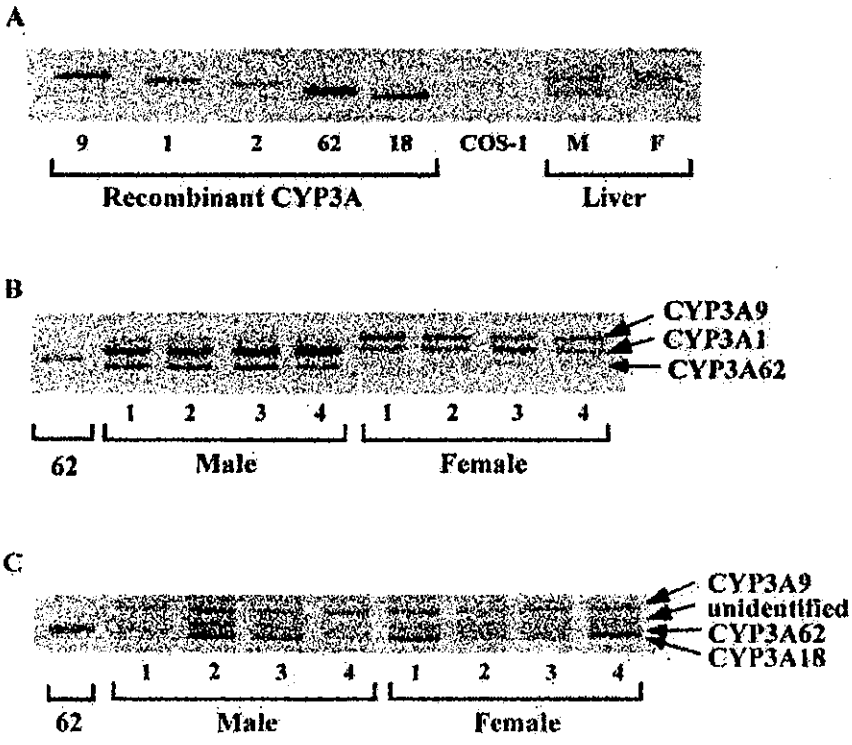

Fig. 4. Western blot analyses of microsomal proteins in rat liver and small intestine. Electrophoresis was performed in a 7.5% SDS-PAGE. The blotted membrane was proved with the anti-CYP3A antibody. Details are described under *Materials and Methods*. A, recombinant CYP3A forms. Lanes: 9, 2 μg of CYP3A9 microsomes; 1, 2 μg of CYP3A1 microsomes; 2, 2 μg of CYP3A2 microsomes; 62, 2 μg of CYP3A62 microsomes; 18, 2 μg of CYP3A18 microsomes; COS-1, 2 μg of COS-1 microsomes; M, 2 μg of microsomes pooled from four male rat livers; F, 2 μg of microsomes pooled from four female rat livers. B, rat liver. Lanes: 62, 4 μg CYP3A62 microsomes; Male, 10 μg male microsomes; Female, 10 μg of female microsomes. C, rat small intestine. Lanes: 62, 6 μg of CYP3A62 microsomes; Male, 50 μg of male microsomes; Female, 50 μg of female microsomes.

not detected in the intestinal tract using real-time PCR. CYP3A18 mRNA was detected as a male-predominant form in the liver and intestinal tract, although the level was very low in the intestinal tract.

After treatment of rats with dexamethasone intraperitoneally, both CYP3A1 and CYP3A2 mRNAs were clearly increased (25 to 200 times) in the liver but not at all in the intestinal tracts as shown in Fig. 2. CYP3A18 mRNA was also enhanced in the liver (about 20 times) and to a lesser extent in the ileum (2–4 times). The expression profile of CYP3A62 mRNA differed from those of CYP3A1, CYP3A2, and CYP3A18 mRNAs. Levels of CYP3A62 mRNA were increased in both liver and intestinal tracts of both sexes (2–30 times) by the treatment. Similar profiles were also detected in the level of CYP3A9 mRNA. These results were confirmed by repeated experiments (data not shown). On the other hand, only CYP3A2 mRNA was strongly increased in the liver of both sexes after treatment with lithocholic acid. In the jejunum of both sexes, CYP3A62 mRNA was increased (2–5 times) by the treatment.

Tissue Distribution of CYP3A62 and Other Rat CYP3A Forms. To assess the tissue distribution of rat CYP3A forms other than liver and intestine, selectively amplified mRNA levels were detected in various tissues by RT-PCR with specific primers as shown in Table 1. The band for CYP3A62 mRNA was found in the stomach of both sexes (Fig. 3). CYP3A9 mRNA was detected in the stomach, lung, and brain of both sexes. CYP3A1 and CYP3A2 mRNAs were also not detected in these tissues. CYP3A18 mRNA was detected in the lungs of both sexes and in the kidney and spleen of the male.

Detection of the CYP3A62 Protein. To characterize the enzymatic properties of a protein derived from CYP3A62 cDNA, all rat CYP3A forms identified were expressed in COS-1 cells as described under *Materials and Methods*. Microsomal proteins in COS-1 cells were immunoblotted by the use of anti-CYP3A antibodies. As shown in Fig. 4A, individual recombinant CYP3A forms expressed in COS-1 cells were clearly separated and detected at different electrophoretic mobilities. The order of those electrophoretic mobilities was CYP3A18, CYP3A62, CYP3A2, CYP3A1, and CYP3A9 from lower dalton registers. The band corresponding to CYP3A62 was detected in the female liver but not clearly in the male liver (Fig. 4B). Bands to CYP3A2 and/or CYP3A1 and CYP3A18 were clearly detected in the male liver, and a band corresponding to CYP3A9 was also detected (Fig. 4B). In livers of female rats, bands of CYP3A1 and CYP3A9 were clearly detected, but not those of CYP3A2 and CYP3A18 (Fig. 4B). In small intestines of both sexes, the bands corresponding to CYP3A62 and CYP3A9 were detected. CYP3A18 was also detected, but the expressed level varied clearly among individuals. An unidentified band was detected in small intestines of both sexes as indicated by the arrow.

Microsomal levels of individual CYP3A forms are summarized in Table 4. Due to overlapping mobilities of CYP3A2 and CYP3A1 in SDS-PAGE, combined amounts are shown for livers of male rats. CYP3A2/CYP3A1 and CYP3A18 had 53.95 and 28.24 pmol/mg protein in male rat livers, respectively. CYP3A9 was 5.12 pmol/mg protein in male rat livers, but CYP3A62 was not clearly quantified (<0.1 pmol/mg protein). On the other hand, CYP3A1 and CYP3A9 had 19.07 and 11.24 pmol/mg protein in female rat livers. CYP3A62 was predominantly detected in female livers (4.81 pmol/mg protein), and CYP3A2 and CYP3A18 in female livers were not detected (<0.1 pmol/mg protein). In small intestines of both sexes, the expressed level of the CYP3A62 was highest among CYP3A forms. The levels of CYP3A62, CYP3A9, and CYP3A18 were quantified at 2.31, 0.78, and 0.84 pmol/mg protein in males, respectively. On the other hand, in females the levels of CYP3A62, CYP3A9, and CYP3A18 were 2.01, 0.73 and 0.89 pmol/mg protein, respectively. Neither CYP3A1 nor CYP3A2 was detected in small intestines of both sexes.

Comparison of Catalytic Activities among Recombinant CYP3A Forms. Testosterone 6β-hydroxylation is known as a typical catalytic activity for CYP3A forms. Some of the members are also known to catalyze 2β- and 15β-hydroxylations of testosterone, although the extent of those activities is lower than that of the 6β-hydroxylation. In the present study, the catalytic property of CYP3A62 was compared with other forms using testosterone hydroxylation. As shown in Table 5B, recombinant CYP3A62 mediated testosterone 6β- and 2β-hydroxylations at the lowest rate (1.14 and 0.06 nmol/min/nmol P450, respectively) among recombinant rat CYP3A forms examined. A catalytic activity of testosterone 16α-hydroxylation (0.76 nmol/min/nmol P450), which could not be detected in CYP3A1, CYP3A2, and CYP3A9, was observed in CYP3A62 as well as in CYP3A18. As shown in Table 5B, CYP3A62 activity was only slightly increased (about 1.3 times) by addition of cytochrome b_5, despite the clear changes in other forms.

To further characterize the drug-metabolizing activity in CYP3A62, catalytic activities of amiodarone and lidocaine *N*-de-ethylations were tested with recombinant rat CYP3A forms. As shown in Table 6, CYP3A62 showed low but clear *N*-de-ethylating activities of both amiodarone and lidocaine (0.007 and 0.054 nmol/min/nmol P450, respectively). In addition, CYP3A9 showed the highest activity of both *N*-de-

TABLE 4

The quantification of CYP3A forms in liver and small intestine of male and female rats. Immunoblot analysis was carried out as described under *Materials and Methods*. The numbers represent the ratio of CYP3A form to microsomal protein (pmol/mg protein). The value represents the mean and the standard deviation of four different rats. <0.10, less than 0.10 pmol/mg protein in liver, and <0.02, less than 0.02 pmol/mg protein in small intestine. The value of CYP3A1 and CYP3A2 forms in male liver represents the total amount of both CYP3A1 and CYP3A2 due to incomplete separation. *, CYP3A62 and CYP3A18 forms were separated incompletely in SDS-PAGE, but the stained band could be divided into two upper (CYP3A62) and lower (CYP3A18) portions by using NIH image 1.59/ppc.

Sex	Tissue	Cytochrome P450				
		CYP3A62	CYP3A1	CYP3A2	CYP3A9	CYP3A18
Male	Liver	<0.10	53.95 ± 4.42		5.12 ± 1.44	28.24 ± 2.29
	Small intestine	2.31 ± 1.33*	<0.02	<0.02	0.78 ± 0.20	0.84 ± 0.82*
Female	Liver	4.81 ± 0.57	11.24 ± 3.29	<0.10	19.07 ± 3.31	<0.10
	Small intestine	2.01 ± 0.33*	<0.02	<0.02	0.73 ± 0.18	0.89 ± 0.50*

TABLE 5

Testosterone hydroxylation by rat recombinant CYP3A forms. The enzyme activity was measured using 50 μg of microsomal protein of COS-1 cells described in detail under *Materials and Methods*. Activities represented are the mean and the standard deviation of three different experiments by nmol/min/nmol P450. 6β-OH, 16α-OH, 2β-OH, and 15β-OH represent the rate of testosterone 6β-, 16α-, 2β-, and 15β-hydroxylase activities, respectively. Cytochrome b_5 (−), without addition of cytochrome b_5; cytochrome b_5 (+), with addition of cytochrome b_5.

A

P450	Testosterone Hydroxylation-Cytochrome b_5 (−)			
	6β-OH	16α-OH	2β-OH	15β-OH
CYP3A62	0.86 ± 0.09	0.61 ± 0.08	0.06 ± 0.00	N.D.
CYP3A1	0.41 ± 0.16	N.D.	0.17 ± 0.01	N.D.
CYP3A2	1.19 ± 0.19	N.D.	0.16 ± 0.01	N.D.
CYP3A9	0.79 ± 0.06	N.D.	0.12 ± 0.00	N.D.
CYP3A18	1.21 ± 0.15	0.44 ± 0.05	0.06 ± 0.00	0.15 ± 0.01

B

P450	Testosterone Hydroxylation-Cytochrome b_5 (+)			
	6β-OH	16α-OH	2β-OH	15β-OH
CYP3A62	1.14 ± 0.16	0.76 ± 0.04	0.06 ± 0.00	N.D.
CYP3A1	2.21 ± 0.19	N.D.	0.48 ± 0.01	N.D.
CYP3A2	10.13 ± 0.91	N.D.	0.46 ± 0.03	N.D.
CYP3A9	2.65 ± 0.19	N.D.	0.19 ± 0.00	N.D.
CYP3A18	3.43 ± 0.56	0.79 ± 0.18	0.12 ± 0.02	0.41 ± 0.06

N.D., not detectable (< 0.02 nmol/min/nmol P450).

TABLE 6

N-De-ethylating activities by rat recombinant CYP3A forms. The enzyme activity was measured using 50 μg of microsomal protein of COS-1 cells described in detail under *Materials and Methods*. Activities represented are the mean and the standard deviation of three different experiments by nmol/min/nmol P450.

P450	Substrate	
	Amiodarone	Lidocaine
CYP3A62	0.008 ± 0.008	0.054 ± 0.012
CYP3A1	0.038 ± 0.005	0.081 ± 0.004
CYP3A2	0.018 ± 0.015	0.174 ± 0.006
CYP3A9	0.156 ± 0.010	0.178 ± 0.007
CYP3A18	0.084 ± 0.008	0.067 ± 0.006

ethylations among rat CYP3A forms (0.156 and 0.178 nmol/min/nmol P450).

Discussion

In our previous experiments with *CYP3A* gene structures, six different *CYP3A* genomic clones were isolated. Four of them were identified to encode exon 1 of the *CYP3A1*, *CYP3A2*, *CYP3A9*, and *CYP3A18* genes, whereas the other two remained unidentified. Based on high similarities of their partial nucleotide sequences and the possible first exon information, a novel rat CYP3A cDNA, CYP3A62 cDNA, has been isolated from a liver cDNA library of a male rat. The entire sequence of the isolated cDNA has 1746 bp and includes an open reading frame of 1491 bp encoding a protein of 497 amino acids. The amino acid number is six residues shorter than those of CYP3A2 and CYP3A9, but it is identical with that of CYP3A18. CYP3A62 showed the highest similarity with CYP3A9 among rat CYP3As and was more similar to human CYP3A4 and CYP3A5 than rat CYP3A1 and CYP3A2 in their amino acid sequences.

CYP3A62 mRNA and CYP3A9 mRNA were detected in the liver and intestinal tract using real-time PCR, and their profiles were similar to one another (Table 3). These profiles were also supported by the quantification of both proteins detected by immunoblot analyses (Fig. 4; Table 4). Another form, CYP3A18, was also detected, but major hepatic forms, CYP3A1 and CYP3A2, were not detected in the intestinal tracts of both sexes (Table 3). This may be related to the difference of catabolic and metabolic activities between livers and small intestines in rats. A large individual variation was observed on the expression level of CYP3A18 protein in the small intestine. The extent of transcriptional activation after the treatment with dexamethasone or lithocholic acid also differs among rat *CYP3A* genes. As shown in Fig. 2, all the CYP3A mRNAs in livers were increased after the treatment of both sexes of rats with dexamethasone. CYP3A1 and CYP3A2 mRNAs were not detected even with real-time PCR in intestines of rats treated with dexamethasone. In contrast, CYP3A62 and CYP3A9 mRNAs were readily detectable and enhanced after dexamethasone treatment in the small intestine and liver. These results clearly indicate the liver-selective expression of CYP3A1 and CYP3A2 and the intestinal-dominant expression of CYP3A62 and CYP3A9. Human CYP3A4 was detected mainly in the liver and intestinal tract and also increased in both tissues after treatment with chemical inducers (Kolars et al., 1992; Goodwin et al., 1999; Schmiedlin-Ren et al., 2001). These expression profiles are more similar to those of CYP3A62 and CYP3A9 than to those of CYP3A1 and CYP3A2. In addition to the expression profile, the nucleotide sequence of the *CYP3A62* proximal promoter region shows higher similarity with that of the *CYP3A4* genes than that of *CYP3A1* and *CYP3A2* genes (Fig. 5). It has been reported that *CYP3A1* and *CYP3A2* genes have hepatocyte nuclear factor-4α (HNF-4α) binding element in their proximal promoter regions (Miyata et al., 1995; Nagata et al., 1999) as shown in Fig. 5. On the other hand, CYP3A62 as well as CYP3A4 do not contain HNF-4α binding element in their proximal promoter regions. Localization of HNF-4α binding site at the proximal promoter region may be associated with the strict liver-specific expression of CYP3A1 and CYP3A2.

Recombinant CYP3A62 mediated testosterone 6β-hydroxylation, but the rate was the lowest among recombinant rat CYP3A forms examined. Microsomal testosterone 6β-hydroxylation of CYP3A62 was slightly enhanced after addition of cytochrome b_5, unlike CYP3A1 and CYP3A2. A profile similar to CYP3A62 on testosterone hydroxylation was observed in that of CYP3A18. As reported, requirement of cytochrome b_5 was dependent on the combination of P450 and substrate (Guengerich, 1983; Schenkman and Jansson, 2003). It may imply that the energy to transfer a second electron from cytochrome b_5 to P450 is different among P450 and/or substrate, but no clear evidence can be provided.

In conclusion, we have isolated a new rat CYP3A form and identified it as CYP3A62 in the present study. Nucleotide sequences of the promoter region and CYP3A62 cDNA exhibited high similarity with the nucleotide sequences of CYP3A4 and CYP3A9 compared with the nucleotide sequences of CYP3A1 and CYP3A2. CYP3A62 was a predominant form in the intestinal tract, whereas CYP3A1 and CYP3A2 were detected only in the liver. In addition, the expression profile of CYP3A62 was also similar to that of CYP3A4 and CYP3A9. Judging from the absence of CYP3A1 and CYP3A2 in the gastrointestinal tract, CYP3A62, as well as CYP3A9 and